Chemical Geology 381 (2014) 243–258

Contents lists available at ScienceDirect

Chemical Geology

journal homepage: www.elsevier.com/locate/chemgeo

Hf–Nd–O isotopic evidence for melting of recycled sediments beneath the Sulu Orogen, North China

Feng Guo [a,*], Weiming Fan [a], Chaowen Li [a], Christina Yan Wang [b], Hongxia Li [a], Liang Zhao [a], Jingyan Li [a,c]

[a] State Key Laboratory of Isotopic Geochemistry, Guangzhou Institute of Geochemistry, Chinese Academy of Sciences, Guangzhou 510640, China
[b] Key Laboratory of Mineralogy and Metallogeny, Guangzhou Institute of Geochemistry, Chinese Academy of Sciences, Guangzhou 510640, China
[c] University of Chinese Academy of Sciences, Beijing 100049, China

ARTICLE INFO

Article history:
Received 22 September 2013
Received in revised form 30 April 2014
Accepted 30 April 2014
Available online 9 May 2014

Editor: L. Reisberg

Keywords:
Recycled sediments
Pudding-cake lithospheric mantle
Hf–Nd–O isotopes
Late Mesozoic
The Sulu Orogen

ABSTRACT

The mantle source of late Mesozoic mafic magmas in the southeastern North China Craton is generally considered to have been enriched by deeply subducted continental lithosphere of the Yangtze Block. The mechanisms through which enrichment occurs are still unclear. Here we document an Early Cretaceous (zircon U–Pb age at 115 ± 2 Ma) dioritic intrusion with some geochemical features similar to sanukitoids (i.e., Al_2O_3 > 17.5%, Ba = 1692–1819 ppm, Sr = 1042–1111 ppm and $\delta^{18}O_{Zircon}$ = 6.2 ± 0.2‰) from the Sulu Orogen in North China. Compared with the regional older (120–130 Ma) mafic magmas (dykes), the diorite has less radiogenic Sr ($^{87}Sr/^{86}Sr(i)$ ~ 0.7075), higher $\varepsilon_{Nd}(t)$ (−9.0 to −8.6) with less radiogenic Hf than Nd ($\Delta\varepsilon_{Hf}(t)$ = −6.1 to −5.2; $\Delta\varepsilon_{Hf}(t) = \varepsilon_{Hf}(t) - 1.36 \times \varepsilon_{Nd}(t) - 2.89$), signatures typically observed from continental zircon-bearing sediments. The primary magma of the dioritic intrusion was probably derived from a mantle enriched by the addition of a significant volume of a restitic component of recycled sediment that had been previously melted to leave residual zircon. Combined Hf–Nd–O isotopic data for the Rushan dioritic intrusion and the earlier mafic rocks requires the involvement of recycled sediments or their melts, incorporated into the lithospheric mantle as lenses or metasomatic veins, to produce a pudding-cake structure beneath the Sulu Orogen.

1. Introduction

Subduction of sediments plays an important role in producing compositional heterogeneity in the mantle and influences the compositions of both subduction-related magmas and oceanic island basalts (OIBs, e.g., White and Patchett, 1984; Othman et al., 1989; Blichert-Toft et al., 1999; Macdonald et al., 2000; Chauvel et al., 2008; Prelević et al., 2013). Geochemical features observed in modern arc basalts, such as large ion lithophile element (LILE) and light REE enrichment, and high field strength element (HFSE) depletion, and isotopic compositions indicating long-term incompatible element enrichment relative to mid-oceanic ridge basalts (MORBs), have been widely considered to reflect a source enriched via the subduction of sediments. Subducted sediment (pelagic and terrestrial sediment) has been also considered as an important component in the mantle sources for some OIBs, such as EMI (enriched mantle 1) and EMII (enriched mantle 2) OIBs (Zindler and Hart, 1986; Weaver, 1991; Hofmann, 1997; Jackson and Dasgupta, 2008). However, the anhydrous and relatively cold nature of subducted continental lithosphere, and the contaminating affects that overlying continental crust might play during magma emplacement, have meant that the roles that subducted sediment might play in the compositional evolution of mantle source regions during continental subduction are significantly less well studied than in the case of oceanic subduction. Nevertheless, investigating such processes could provide insights into crustal recycling processes, enrichment of continental mantle lithosphere and the origin of post-orogenic mafic magmatism.

The Dabie–Sulu high- to ultrahigh-pressure (HP–UHP) metamorphic belt is now recognized as the Triassic collisional belt between the North China Craton (NCC) and the Yangtze Block (e.g., Li et al., 1993). The preservation in this belt of HP–UHP minerals such as coesite and diamond as inclusions in eclogites suggests that continental crust itself was subducted to mantle depths of >200 km (e.g., Xu et al., 1992; Ye et al., 2000). The range of UHP protoliths spans from ultramafic peridotite, mafic eclogite, orthogneiss and paragneiss to marble (Zheng et al., 2003 and references therein; Proyer et al., 2013), and indicates that the northern part of the Yangtze continental lithosphere (including the mantle and crust sections) was entirely subducted beneath the NCC. This subducted material interacted with the overlying NCC lithospheric mantle to form an enriched mantle source component that subsequently contributed to regional mafic to ultramafic magmatism from Late Triassic to Early Cretaceous (e.g., Zhang et al., 2002; Fan et al., 2004; Guo et al., 2004; Zhao et al., 2012; Ma et al., 2014). Indeed, numerous Sr–Nd isotopic studies on Late Triassic to Early Cretaceous mafic

* Corresponding author. Tel.: +86 20 85290280; fax: +86 20 85290130.
E-mail address: guofengt@263.net (F. Guo).

http://dx.doi.org/10.1016/j.chemgeo.2014.04.028
0009-2541/

magmas have identified a significant component with isotopic composition similar to EMII in the source of magmas related to the Sulu Orogen (e.g., Guo et al., 2004; Yang et al., 2004; Zhao et al., 2012; Ma et al., 2014). However, debate continues as to how mantle enrichment occurred, with suggested mechanisms including both slab-fluid and slab-melt mediated enrichments variably involving a lithospheric mantle sandwiched between overlying crust and underlying subducted continental crust (e.g., Fan et al., 2004; Dai et al., 2011).

In this paper, we present the results of a comprehensive *in situ* zircon U–Pb–Hf–O–REE, whole-rock geochemical and Sr–Nd–Hf isotopic study on an Early Cretaceous dioritic intrusion from the Rushan area of the Sulu Orogen, which shows some geochemical features of sanukitoids — high-Mg andesites or diorites that are widely distributed in Archean terranes and are interpreted to be derived from a peridotite mantle (Tatsumi and Ishizaka, 1982; Shirey and Hanson, 1984; Martin et al., 2005). For comparison, we also present new whole-rock geochemical and Sr–Nd–Hf isotopic data for the earlier mafic dykes (120–130 Ma) in the region as well as published data for the well-studied Fangcheng basalts (~125 Ma) extruded onto the southeastern margin of the NCC (e.g., Zhang et al., 2002; Guo et al., 2013b). These rocks show differing degrees of Hf–Nd decoupling and $\delta^{18}O$ enrichment, which are best interpreted in terms of derivation from a lithospheric mantle variably enriched via a continental sediment component. This component was most likely derived from the subducted continental Yangtze Block. The long-term preservation of the subducted sediment component within the lithospheric mantle supports the existence of pudding-cake lithospheric mantle beneath the Sulu Orogen of the NCC, and provides important information regarding the regional crust–mantle architecture and mantle-modification processes involved in continental subduction.

2. Geological background

The Sulu Orogen forms the eastern extent of the Triassic Qinling–Dabie collisional belt (Fig. 1), where HP–UHP rocks are widely distributed (Fig. 1a, Ye et al., 2000; Zheng et al., 2003). The ENE-trending Wulian–Qingdao–Yantai fault (WQYF — Fig. 1a) juxtaposes mainly Late Archean to Early Proterozoic high-grade metamorphic rocks of the NCC and the Mesozoic Laiyang Basin, to the north and west, against the Neoproterozoic low-grade metamorphic complexes and interleaved Triassic HP–UHP rocks, to the south. Based on zircon U–Pb–Hf isotope data, Zhou et al. (2008a,b,c, 2012) identified the metamorphic rocks of both NCC and Yangtze affinity at the northern margin of the Sulu Orogen, with the Haizhou and Wulian metamorphic complexes to be of Yangtze affinity, whereas the Penglai, Fenzishan and Jingshan metamorphic complexes were of NCC affinity. They further considered that the surface boundary between the Yangtze Block and NCC was located along the Baichihe–Yantai fault (Zhou et al., 2012). The occurrence of HP–UHP rocks, voluminous Late Mesozoic granitoid plutons and mafic dykes, as well as the association with large-scale gold mineralization, makes this an important region for studying orogenic processes of continental subduction, crust–mantle interaction processes, and their influence on economic mineralization.

The Rushan area is located in the eastern Sulu Orogen. A dioritic intrusion forms a ~2 km^2 outcrop near the East Sea (Fig. 1a). All samples are of fresh pyroxene diorite. The fine- to medium-grained assemblage comprises clinopyroxene (5–8%), hornblende (25–30%), plagioclase (50–60%), biotite (3–5%) and quartz (5–10%) with accessory ilmenite, zircon and apatite. The studied mafic dykes include lamprophyres and dolerites and their petrological features have been reported by Guo et al. (2004) and Ma et al. (2014). They contain phenocrysts of K-feldspar (0.8–2 mm) for lamprophyres or plagioclase (1–3 mm) for dolerites, hornblende (0.5–2 mm), biotite (0.5–3 mm) clinopyroxene (0.5–2 mm), and sometimes minor olivine (0.5–1.5 mm), in a groundmass of fine-grained plagioclase, alkali feldspar, biotite, clinopyroxene and minor autogenetic carbonates and accessory apatite and opaque oxides. The Fangcheng basalt was erupted west of the Tan–Lu fault. These rocks are high-MgO (8–12%) olivine basalts, with olivine and clinopyroxene phenocrysts set in a matrix of olivine and pyroxene microcrystallines and glass (Zhang et al., 2002; Guo et al., 2013b).

3. Analytical techniques

3.1. In situ O–U–Pb–Hf isotope and REE analyses on zircon

The zircons were separated from sample 09SD-111 using conventional methods. They were then handpicked under a binocular microscope, mounted in epoxy resin with zircon standards 91500 and Penglai and polished to about half thickness. The *in situ* oxygen isotope analysis was done using a Secondary Ion Microprobe Spectrometer (SIMS) Cameca ims-1280 at the Institute of Geology and Geophysics (IGG), Chinese Academy of Sciences (CAS). The Cs^+ primary beam was accelerated at 10 kV with an intensity of ca. 2 nA. The spot size was about 20 μm in diameter (10 μm beam diameter + 10 μm raster). An electron gun was used to compensate for sample charging during analysis. Secondary ions were extracted with a −10 kV potential. Oxygen isotopes were measured in multi-collector mode with two off-axis Faraday cups with each analysis consisting of 4 × 20 cycles of ion counting. The O isotope results are reported in the conventional $\delta^{18}O$ notation relative to the reference standard VSMOW. External reproducibility of zircon standards was typically better than 0.4‰ (2 SD) for $\delta^{18}O$. Detailed description of the analytical procedure was reported in Li et al. (2010) and Guo et al. (2013a). During analysis, the Penglai and 91500 zircon standards respectively yield $\delta^{18}O = 5.30 \pm 0.11‰$ (n = 29) and $\delta^{18}O = 9.92 \pm 0.29‰$ (n = 20).

By the same mount as for O isotope analyses, *in situ* simultaneous determination of U–Pb and Hf isotopes and REE concentrations of zircons were done by an Agilent 7500a Q-ICPMS and a Neptune MC-ICPMS coupled with a 193 nm laser ablation system at the IGG, CAS. The detailed analytical method was reported in Xie et al. (2008). Spot laser ablation was adopted in this study with spot diameters of 50–60 μm and laser pulse repetition frequencies of 6–8 Hz. The zircon U–Pb isotopic ratio was corrected by using zircon 91500 as an external standard. Fractionation correction and results were calculated using GLITTER (ver 4.0, Knudsen et al., 2001). The results were calculated using the Isoplot program (ver. 2.49) (Ludwig, 2001). For zircon Hf isotopes, raw count rates for ^{172}Yb, ^{173}Yb, ^{175}Lu, $^{176}(Hf + Yb + Lu)$, ^{177}Hf, ^{178}Hf, ^{179}Hf, ^{180}Hf and ^{182}W were collected. ^{175}Lu was used for interference correction of ^{176}Lu on ^{176}Hf. The $^{176}Yb/^{172}Yb$ value of 0.5887 and mean β_{Yb} value obtained during Hf analysis on the same spot were applied for the interference correction of ^{176}Yb on ^{176}Hf (Wu et al., 2006). During analysis, the $^{176}Hf/^{177}Hf$ ratios of the standard zircons 91500 and TEMORA were 0.282305 ± 14 (2σ, n = 30) and 0.282684 ± 30 (2σ, n = 15), respectively. The *in situ* U–Pb–Hf–O isotopic compositions and REE concentrations of zircons from the Rushan dioritic intrusion are listed in Table 1.

3.2. Whole-rock major, trace element and Sr–Nd–Hf isotope analyses

All samples for whole-rock major oxides, trace elements and Sr–Nd–Hf isotope analyses were crushed and fresh chips were picked and washed in 0.05 N HCl and purified water. The cleaned chips then were ground in an agate mortar to less than 200 mesh. Whole-rock major oxides were determined by X-ray fluorescence (XRF) spectrometry on fused glass pellets at the Guangzhou Institute of Geochemistry (GIG), CAS. Precision of the XRF analyses is estimated to be 2%.

Trace elements were determined by ICP-MS at the Institute of Geochemistry, CAS. The powders (~50 mg) were digested in 1 ml HF and 0.5 ml of HNO_3 in Teflon cups sealed in screw-top stainless steel bombs at 190 °C for 12 h. The analytical precision is generally better than 5% for elements with concentrations >200 ppm, and 5–10% when less than 200 ppm. Detailed description of the analytical procedure was reported in Qi et al. (2000). The analytical results of major oxides

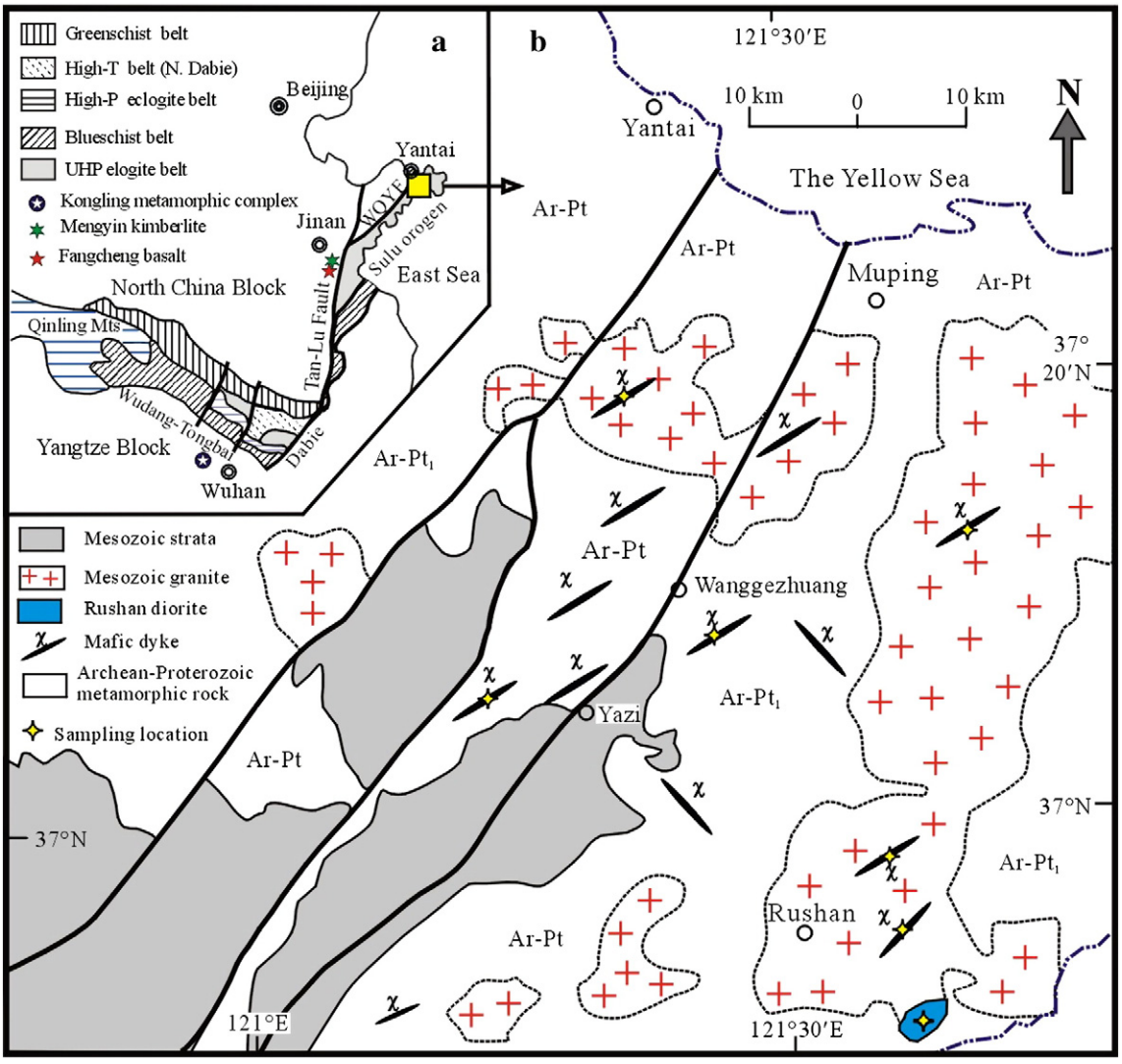

Fig. 1. Geological map of the Sulu Orogen showing the distribution of the Rushan dioritic intrusion and the related mafic dykes. Modified after Guo et al. (2004).

and trace elements of several international standards are listed in the Appendix.

Sr and Nd isotopic analysis was performed on a Neptune multi-collector ICP-MS at GIGCAS, using analytical procedures described by Li et al. (2006). Powders were dissolved in HF-$HClO_4$ and the dissolution was at 200 °C for a week. Sr and Nd were separated using conventional ion exchange columns, and the Nd fractions were further separated by HDEHP-coated Kef columns. The measured $^{87}Sr/^{86}Sr$ and $^{143}Nd/^{144}Nd$ ratios were normalized to $^{86}Sr/^{88}Sr = 0.1194$ and $^{146}Nd/^{144}Nd = 0.7219$, respectively. The reported $^{87}Sr/^{86}Sr$ and $^{143}Nd/^{144}Nd$ ratios were adjusted to the NBS SRM 987 standard ($^{87}Sr/^{86}Sr = 0.710247 \pm 8$, 2σ) and the JNdi-1 standard ($^{143}Nd/^{144}Nd = 0.512115 \pm 4$, 2σ), respectively. Ten analyses of rock standard BHVO-2 yield $^{87}Sr/^{86}Sr = 0.703496 \pm 6$ (2σ, n = 10) and ten analyses of rock standard BHVO-2 and JB-3 give $^{143}Nd/^{144}Nd = 0.512965 \pm 4$ (2σ, n = 10) and $^{143}Nd/^{144}Nd = 0.513041 \pm 5$ (2σ, n = 10), respectively. The procedural blanks were <200 pg for Sr, and ~30 pg for Nd. For Hf isotopic analysis, about 0.5 g sample powders and 1.0 g $Li_2B_4O_7$ were mixed homogeneously. The mixtures were fused in Pt crucibles at 1250 °C for 15 min in a high-frequency furnace. Then about 400 mg of the resulting glassy samples were dissolved in 2 N HCl. Hf fraction was separated by using a modified single-column separation procedure by ion exchange using Ln-Spec resin. A detailed analytical procedure was reported in Li et al. (2006). Hf isotopes are determined using a Finnigan Neptune MC-ICP-MS at GIGCAS. The $^{176}Hf/^{177}Hf$ ratios were normalized to $^{179}Hf/^{177}Hf = 0.7325$. During Hf isotope analyses, the reported $^{176}Hf/^{177}Hf$ ratios were adjusted to the standard solution JMC-475 (0.282163 ± 7, 2σ). Ten analyses of USGS reference material BHVO-2 yield $^{176}Hf/^{177}Hf = 0.283087 \pm 10$ (2σ, n = 10) and five analyses of JB-3 give $^{176}Hf/^{177}Hf = 0.283222 \pm 10$ (2σ, n = 5), respectively. The procedural blanks were ~50 pg for Hf. The whole-rock major and trace element compositions and Sr–Nd–Hf isotopic compositions of the Rushan dioritic intrusion and the studied mafic dykes as well as the previously published Fangcheng basalts (Guo et al., 2013b) are listed in Table 2.

4. Results

4.1. Zircon U–Pb age, Hf–O isotope and REE compositions of the Rushan diorites

The zircons from the Rushan diorite samples yield a weighted mean $^{238}U/^{206}Pb$ age of 115 ± 2 Ma (MSWD = 0.93, n = 24, Fig. 2a). They are magmatic in origin, having LREE-depleted and HREE-enriched REE patterns with Ce/Ce* of 4 to 70 and Eu/Eu* of 0.30 to 0.39 that suggest zircon crystallization after plagioclase fractionation in a relatively oxidized magma (Fig. 2b). *In situ* Hf isotopic analyses

Table 1
U–Pb–Hf–O isotopic compositions and REE contents of zircon from the Rushan diorite (09SD-111), Sulu Orogen.

Spot	Th	U	$^{207}Pb/^{235}U$	1σ	$^{206}Pb/^{238}U$	1σ	$^{207}Pb/^{235}U$ Age (Ma)	1σ	$^{206}Pb/^{238}U$ Age (Ma)	1σ	$^{207}Pb/^{206}Pb$ Age (Ma)	1σ	La	Ce	Pr	Nd	Sm	Eu
A-1	105	135	0.12	0.0085	0.0179	0.0006	111	5	115	2	181	40	0.04	11.81	0.07	1.01	1.64	0.39
A-2	332	211	0.13	0.0047	0.0184	0.0004	120	4	117	2	165	51	0.16	14.48	0.66	7.26	9.60	2.01
A-3C	635	344	0.12	0.0039	0.0175	0.0003	111	4	112	2	101	44	0.53	13.57	0.12	2.13	3.42	0.80
A-3R																		
A-4	526	305	0.12	0.0052	0.0176	0.0004	116	5	112	3	188	58	0.13	20.95	0.71	9.98	20.27	3.94
A-5	266	190	0.12	0.0023	0.0179	0.0003	116	2	115	2	149	21	0.18	16.96	0.79	8.39	13.71	2.77
A-6c	290	200	0.12	0.0024	0.0185	0.0003	117	2	118	2	99	21	0.10	14.96	0.49	6.25	7.49	1.50
A-7	108	99	0.12	0.0033	0.0176	0.0003	114	3	112	2	146	34	0.16	15.86	0.72	8.40	9.53	1.89
A-8	390	246	0.12	0.0020	0.0182	0.0003	116	2	116	2	115	18	0.15	16.54	0.76	8.58	10.50	2.21
A-9	516	303	0.12	0.0019	0.0184	0.0003	119	2	117	2	144	16	0.02	12.31	0.16	2.15	3.41	0.65
A-10	743	382	0.12	0.0017	0.0184	0.0003	117	2	117	2	114	15	0.18	20.33	0.83	10.32	18.37	3.91
A-11C	67	70	0.12	0.0046	0.0177	0.0004	112	4	113	2	90	54	0.18	19.89	0.81	9.73	17.78	4.01
A-11R																		
A-12	263	179	0.12	0.0027	0.0176	0.0003	116	2	112	2	188	25	0.02	10.03	0.08	1.15	2.01	0.48
A-13	118	101	0.12	0.0038	0.0176	0.0003	117	3	113	2	202	40	0.15	16.15	0.80	9.39	11.54	2.25
A-14	86	83	0.12	0.0053	0.0175	0.0004	114	5	112	3	150	63	0.05	11.84	0.31	4.14	5.26	1.10
A-15C	119	102	0.12	0.0061	0.0174	0.0004	119	5	111	3	285	66	0.02	9.98	0.07	1.28	2.57	0.63
A-15R																		
A-16	124	117	0.12	0.0056	0.0174	0.0004	115	5	111	3	203	63	0.44	15.86	0.31	2.96	3.24	0.60
A-17R	416	256	0.12	0.0034	0.0182	0.0003	118	3	116	2	165	34	0.15	15.70	0.71	8.66	10.96	2.36
A-17R																		
A-18	713	358	0.12	0.0019	0.0183	0.0003	119	2	117	2	157	16	0.26	27.16	0.97	13.90	22.79	4.59
A-19	278	205	0.12	0.0030	0.0179	0.0003	118	3	114	2	204	28	0.13	15.97	0.72	8.68	9.47	1.89
A-20C	120	99	0.12	0.0044	0.0180	0.0004	116	4	115	2	142	48	0.04	13.52	0.39	5.42	6.91	1.41
A-20R																		
A-21	108	93	0.12	0.0037	0.0179	0.0003	117	3	114	2	173	38	0.02	12.24	0.18	3.09	4.93	1.03
A-22	416	267	0.12	0.0039	0.0179	0.0003	118	3	115	2	192	39	0.18	19.76	0.88	10.82	14.06	2.98
A-23	110	101	0.12	0.0056	0.0182	0.0004	118	5	116	3	147	63	0.11	11.75	0.24	3.12	4.80	0.97
A-24	186	142	0.12	0.0036	0.0177	0.0003	114	3	113	2	125	39	0.05	16.76	0.54	7.80	10.67	2.05

Spot	Gd	Tb	Dy	Ho	Er	Tm	Yb	Lu	Eu/Eu*	Ce/Ce*	$^{176}Yb/^{177}Hf$	2σ	$^{176}Lu/^{177}Hf$	2σ	$^{176}Hf/^{177}Hf \pm 2\sigma$	$\varepsilon_{Hf}(t)$	T_{DM} (Ma)	$\delta^{18}O$ (‰)	2σ
A-1	7.39	2.53	26.2	9.88	40.0	9.55	90.9	19.22	0.34	54	0.01609	1.14E−04	0.00061	4.0E−06	0.282359 ± 17	−12.1	1262	5.74	0.24
A-2	37.12	10.88	100.4	35.76	133.4	27.58	235.5	46.55	0.33	10	0.02874	8.37E−04	0.00105	3.1E−05	0.282388 ± 20	−11.1	CB	5.64	0.41
A-3C	11.45	3.54	31.9	11.55	44.5	9.85	90.0	18.57	0.39	13	0.01145	3.74E−05	0.00044	1.6E−06	0.282334 ± 17	−13.0	1291	6.35	0.36
A-3R																		6.27	0.34
A-4	73.08	21.46	190.4	64.42	234.4	48.67	414.9	78.80	0.31	16	0.03983	3.78E−04	0.00145	1.3E−05	0.282346 ± 20	−12.6	1308	6.08	0.25
A-5	59.09	17.12	152.1	52.22	192.5	39.90	338.0	65.19	0.30	11	0.01789	1.10E−04	0.00065	4.3E−06	0.282353 ± 20	−12.4	1272	6.27	0.35
A-6c	28.40	8.84	82.0	29.47	113.0	24.20	214.4	42.48	0.31	16	0.01936	5.69E−05	0.00072	1.6E−06	0.282341 ± 21	−12.8	1291	6.01	0.41
A-6r																		5.97	0.47
A-7	35.60	10.83	101.4	35.94	136.7	28.59	248.3	48.78	0.31	11	0.02828	1.51E−04	0.00105	5.9E−06	0.282372 ± 22	−11.7	1258	6.62	0.34
A-8	44.56	13.50	127.1	45.03	170.1	35.32	304.9	59.54	0.31	11	0.01484	5.09E−05	0.00056	9.3E−07	0.282360 ± 24	−12.1	1259	5.90	0.29
A-9	12.62	3.77	36.4	12.84	49.9	11.10	100.3	19.60	0.30	52	0.01039	1.08E−04	0.00039	3.7E−06	0.282363 ± 22	−12.0	1249	6.02	0.31
A-10	76.18	21.61	196.2	66.49	246.4	50.02	430.9	82.28	0.32	12	0.02314	7.32E−05	0.00085	2.4E−06	0.282420 ± 31	−10.0	1184	5.53	0.49
A-11C	81.52	23.70	218.5	73.72	273.7	55.08	473.3	88.68	0.32	12	0.03608	3.21E−05	0.00133	1.2E−06	0.282314 ± 22	−13.8	1350	6.64	0.33
A-11R											0.05517	3.12E−04	0.00069	4.6E−07	0.282314 ± 21	−13.7	1327	6.59	0.25
A-12	8.26	2.63	26.5	9.53	39.3	8.87	83.0	17.04	0.36	67	0.04655	6.24E−05	0.00195	1.3E−05	0.282443 ± 27	−9.3	1186	5.43	0.27
A-13	42.62	12.01	112.1	38.38	144.5	30.13	266.9	51.10	0.31	11	0.00839	2.56E−05	0.00169	1.9E−06	0.282366 ± 24	−12.0	1289	6.59	0.26
A-14	17.62	5.26	49.3	17.15	68.0	14.78	134.0	27.01	0.35	22	0.02574	3.55E−04	0.00033	8.4E−07	0.282390 ± 24	−11.0	1209	6.45	0.44
A-15C	11.75	3.85	38.3	13.74	56.5	12.23	112.7	22.54	0.35	70	0.01986	1.14E−04	0.00096	1.3E−05	0.282371 ± 22	−11.7	1256	5.87	0.40
A-15R																		5.94	0.26
A-16	11.68	3.37	32.6	11.73	47.3	10.52	99.5	20.11	0.30	10	0.01311	1.05E−04	0.00075	4.4E−06	0.282371 ± 19	−11.7	1250	5.96	0.24
A-17R	49.44	14.53	141.0	49.15	190.1	38.70	336.4	66.04	0.31	11	0.01093	9.54E−05	0.00050	3.9E−06	0.282328 ± 18	−13.2	1301	6.54	0.41
A-17R											0.00971	7.56E−05	0.00066	2.4E−06	0.282337 ± 22	−12.9	1294	6.59	0.23
A-18	87.00	24.40	224.5	74.10	278.3	55.78	485.4	89.01	0.31	13	0.04314	6.09E−05	0.00041	3.3E−06	0.282341 ± 24	−12.7	1280	6.04	0.27
A-19	34.69	10.03	96.9	33.96	132.6	27.29	243.9	47.21	0.32	12	0.02043	6.45E−04	0.00037	2.5E−06	0.282323 ± 26	−13.4	1304	6.05	0.35
A-20C	22.65	6.35	58.9	19.64	76.4	16.12	148.2	28.70	0.34	25	0.02732	2.63E−05	0.00159	3.2E−06	0.282361 ± 23	−12.1	1292	6.54	0.27
A-20R																		6.47	0.44
A-21	18.24	5.32	51.7	17.91	69.9	15.00	136.9	26.62	0.33	50	0.01222	6.48E−05	0.00073	2.2E−05	0.282332 ± 28	−13.1	1303	6.44	0.24
A-22	56.12	16.26	150.1	50.55	195.4	39.72	354.4	65.86	0.32	12	0.01364	4.67E−05	0.00102	1.2E−06	0.282375 ± 25	−11.6	1253	6.35	0.29
A-23	16.44	4.87	46.8	16.18	66.5	13.93	130.7	25.59	0.33	17	0.01783	6.39E−05	0.00046	2.2E−06	0.282337 ± 24	−12.9	1287	6.41	0.40
A-24	32.70	8.84	83.0	27.64	107.0	22.35	200.5	38.16	0.33	23	0.019	1.00E−05	0.00051	1.9E−06	0.282296 ± 21	−14.4	1346	6.70	0.29

Note: C — core portion of zircon; R — rim of zircon.

Table 2
Major oxide (wt.%), trace element (ppm) and Sr–Nd–Hf isotopic compositions of Rushan diorite samples and other mafic rocks in the southeastern NCC.
Vervoort et al. (1999).

Sample	Locality	geographic coordinates	Rock type	Age (Ma)	SiO_2	TiO_2	Al_2O_3	Fe_2O_3	MnO	CaO	MgO	Na_2O	K_2O	P_2O_5	LOI	Total	Mg#	Sc	V	Cr	Co	Ni
09SD-106	Rushan	36°51.42′N 120°42.62′E	Diorite	115	56.85	0.80	17.63	7.05	0.12	6.13	3.37	3.84	2.95	0.47	0.39	99.60	46.2	14	143	75	18	16
09SD-107	Rushan		Diorite	115	56.83	0.81	17.64	7.10	0.12	6.14	3.41	3.84	2.85	0.47	0.53	99.74	46.4	14	148	88	17	21
09SD-108	Rushan		Diorite	115	57.09	0.86	17.50	7.04	0.11	5.93	3.42	3.71	3.25	0.43	0.45	99.79	46.6	15	148	55	17	17
09SD-109	Rushan		Diorite	115	56.99	0.81	17.60	7.04	0.12	6.08	3.35	3.83	3.00	0.46	0.55	99.84	46.2	14	142	57	16	16
09SD-110	Rushan		Diorite	115	57.13	0.79	17.63	6.96	0.12	6.02	3.31	3.84	3.08	0.45	0.28	99.62	46.1	13	140	46	16	11
09SD-76	Jiaodong	37°10.06′N 121°28.07′E	Mafic dyke	120	48.85	0.80	14.06	7.77	0.12	7.68	9.50	2.22	1.94	0.29	6.69	99.92	68.8	20	153	544	35	152
09SD-78	Jiaodong		Mafic dyke	120	48.94	0.78	14.08	7.73	0.12	7.64	9.40	2.28	1.99	0.29	6.66	99.90	68.6	20	154	546	36	153
09SD-80	Jiaodong		Mafic dyke	120	48.43	0.90	13.34	8.31	0.13	8.64	10.84	2.20	2.22	0.45	4.21	99.68	70.1	23	170	575	41	233
09SD-81	Jiaodong		Mafic dyke	120	48.71	0.93	13.95	8.07	0.13	8.60	9.51	2.41	2.34	0.47	4.61	99.72	68.0	22	168	471	37	183
09SD-82	Jiaodong		Mafic dyke	120	48.52	0.91	13.72	8.11	0.13	8.66	10.02	2.23	2.38	0.46	4.59	99.72	69.0	22	168	526	39	210
09SD-84	Jiaodong		Mafic dyke	120	48.35	0.92	13.89	8.14	0.13	8.50	9.79	2.25	2.31	0.47	5.01	99.75	68.4	22	170	508	37	193
09SD-85	Jiaodong		Mafic dyke	120	48.42	0.91	13.50	8.19	0.12	8.59	10.36	2.16	2.28	0.46	4.73	99.73	69.5	22	166	515	38	206
09SD-86	Jiaodong		Mafic dyke	120	48.49	0.93	13.81	8.21	0.13	8.34	10.01	2.39	2.25	0.47	4.71	99.72	68.7	21	166	493	39	204
09SD-90	Jiaodong	37°08.18′N 121°21.80′E	Mafic dyke	120	53.48	0.75	14.13	6.85	0.13	6.53	8.21	2.34	2.86	0.44	3.94	99.65	68.3	17	132	484	29	165
09SD-91	Jiaodong		Mafic dyke	120	53.09	0.74	15.05	6.86	0.13	7.42	6.65	3.03	2.03	0.38	4.34	99.71	63.6	21	142	400	28	89
09SD-94	Jiaodong		Mafic dyke	120	52.72	0.70	14.19	7.43	0.15	7.09	8.62	2.35	2.12	0.35	3.95	99.68	67.6	20	140	594	31	170
09SD-96	Jiaodong		Mafic dyke	120	53.54	0.72	14.63	7.26	0.14	6.57	8.14	2.52	2.49	0.37	3.24	99.61	66.8	19	141	520	27	134
09SD-98	Jiaodong	37°07.75′N 121°25.87′E	Mafic dyke	120	52.65	0.86	15.56	7.57	0.12	6.73	7.27	3.10	1.86	0.34	3.59	99.64	63.3	18	143	363	31	144
09SD-103	Jiaodong	37°08.05′N 121°25.62′E	Mafic dyke	120	46.23	0.97	13.06	7.78	0.13	7.84	9.30	2.41	3.59	0.50	7.88	99.67	68.3	20	150	518	33	188
09SD-105	Jiaodong		Mafic dyke	120	46.30	0.97	13.40	8.24	0.13	8.44	9.62	2.51	3.22	0.48	6.16	99.49	67.7	21	163	513	36	199
09SD-165	Fangcheng	35°16.66′N 118°09.49′E	Basalt	125	49.57	1.13	14.50	8.77	0.13	8.36	8.73	2.40	2.86	0.96	2.16	99.57	64.2	16	155	369	34	130
09SD-167	Fangcheng		Basalt	125	49.57	1.12	14.46	8.83	0.13	8.37	8.94	2.37	2.79	0.93	2.06	99.58	64.6	17	153	355	34	118
09SD-169	Fangcheng		Basalt	125	49.38	1.13	14.34	8.78	0.13	8.54	8.80	2.92	1.68	0.95	2.97	99.62	64.3	18	153	370	34	125
09SD-171	Fangcheng	35°16.72′N 118°09.73′E	Basalt	125	48.30	1.13	12.17	8.79	0.13	10.13	11.91	2.72	0.85	0.74	2.71	99.58	70.9	22	167	613	43	256
09SD-172	Fangcheng		Basalt	125	48.02	1.12	12.25	8.52	0.12	10.43	11.19	2.56	0.90	0.74	3.81	99.67	70.3	21	167	589	42	255
09SD-177	Fangcheng		Basalt	125	47.49	1.13	12.51	8.93	0.13	9.41	11.92	2.61	0.96	0.77	3.81	99.67	70.6	20	161	540	41	228
09SD-178	Fangcheng		Basalt	125	49.28	1.15	14.47	8.70	0.12	8.51	7.90	3.36	1.65	0.96	3.55	99.64	62.0	18	153	357	33	122
09SD-179	Fangcheng		Basalt	125	45.18	1.05	11.98	8.22	0.13	11.89	11.36	2.48	0.87	0.73	5.94	99.85	71.3	20	160	497	39	209
09SD-183	Fangcheng		Basalt	125	47.87	1.13	12.89	8.86	0.13	9.25	11.20	2.83	1.03	0.79	3.70	99.68	69.5	20	160	509	39	214
09SD-185	Fangcheng		Basalt	125	47.36	1.13	12.68	8.91	0.14	9.33	11.70	2.64	0.95	0.80	4.04	99.68	70.3	20	164	541	40	222

Sample	Rb	Sr	Y	Zr	Hf	Nb	Ta	Ba	La	Ce	Pr	Nd	Sm	Eu	Gd	Tb	Dy	Ho	Er	Tm	Yb	Lu	Th	U
09SD-106	65.9	1093	20.2	124	3.16	10.8	0.61	1819	59.4	110.2	12.9	49.1	8.85	2.29	7.35	0.90	4.03	0.79	2.11	0.28	1.76	0.25	8.54	1.94
09SD-107	64.0	1111	21.3	116	2.96	11.6	0.66	1790	59.7	111.1	13.1	49.7	8.73	2.24	7.28	0.87	4.18	0.81	2.23	0.29	1.83	0.27	9.33	2.20
09SD-108	77.4	1042	21.6	157	3.74	13.5	0.83	1692	59.5	111.2	13.0	49.6	8.66	2.28	7.20	0.86	4.17	0.80	2.26	0.30	1.94	0.27	10.75	2.61
09SD-109	64.2	1064	20.3	120	3.16	10.9	0.62	1775	58.6	108.5	12.6	48.0	8.44	2.24	7.19	0.85	4.01	0.78	2.09	0.27	1.81	0.27	9.01	2.00
09SD-110	66.3	1069	20.5	141	3.50	11.6	0.66	1751	58.2	108.3	12.7	47.7	8.39	2.28	6.99	0.86	3.98	0.77	2.10	0.28	1.75	0.26	8.96	1.98
09SD-76	45.8	783	16.7	134	3.30	6.0	0.40	1388	54.0	100.0	11.4	42.1	6.75	1.75	5.72	0.70	3.41	0.69	1.94	0.27	1.64	0.25	7.59	1.16
09SD-78	46.1	815	16.6	136	3.25	6.1	0.36	1416	54.7	101.6	11.4	41.0	6.77	1.75	5.79	0.69	3.39	0.70	1.97	0.26	1.64	0.23	7.77	1.18
09SD-80	42.1	939	19.9	154	3.68	8.9	0.55	2056	74.3	139.1	16.1	59.4	9.47	2.34	7.96	0.93	4.13	0.84	2.30	0.29	1.85	0.27	9.51	1.58
09SD-81	45.2	985	20.0	159	3.69	9.4	0.57	2090	75.9	140.2	16.3	59.9	9.82	2.35	7.95	0.93	4.22	0.86	2.33	0.29	1.95	0.27	9.83	1.59
09SD-82	47.5	996	20.2	157	3.75	9.3	0.53	1951	75.1	140.3	16.2	59.3	9.48	2.48	7.68	0.95	4.22	0.84	2.33	0.30	1.85	0.28	9.51	1.55
09SD-84	43.7	998	19.5	155	3.69	9.0	0.54	1830	72.8	137.0	16.0	57.7	9.32	2.36	7.68	0.94	4.03	0.82	2.34	0.29	1.85	0.27	9.45	1.59
09SD-85	42.1	971	19.1	151	3.73	8.9	0.52	1806	73.6	137.6	15.9	59.3	9.54	2.35	7.88	0.93	4.15	0.80	2.36	0.28	1.84	0.26	9.29	1.52
09SD-86	40.2	954	19.8	159	3.69	9.1	0.61	1796	75.3	141.2	16.3	59.8	9.61	2.38	7.98	0.91	4.03	0.84	2.31	0.29	1.84	0.27	9.66	1.60
09SD-90	60.7	850	14.5	149	3.99	10.3	0.69	3281	43.5	85.6	10.1	38.4	6.58	1.61	6.05	0.66	3.02	0.60	1.70	0.21	1.40	0.21	9.76	1.56

09SD-91	48.9	918	17.8	159	4.04	8.7	0.54	2537	51.6	96.2	11.2	41.4	6.76	1.85	6.50	0.73	3.65	0.75	2.08	0.26	1.78	0.25	7.23	1.41
09SD-94	49.1	840	16.2	155	3.66	8.3	0.54	1751	46.2	88.0	10.0	37.4	6.30	1.58	5.74	0.67	3.23	0.66	1.91	0.26	1.58	0.23	7.03	1.27
09SD-96	53.0	913	16.4	153	3.51	8.3	0.60	2525	48.7	88.1	9.8	35.5	5.70	1.47	4.98	0.63	3.06	0.63	1.74	0.23	1.54	0.22	6.62	1.21
09SD-98	36.7	1046	15.9	156	3.86	8.2	0.49	2369	44.5	80.1	9.1	33.9	5.57	1.49	5.15	0.61	3.10	0.60	1.75	0.22	1.43	0.21	5.93	1.02
09SD-103	92.4	1458	18.7	187	4.42	14.0	0.73	3278	76.2	137.1	15.9	57.9	8.86	2.17	7.21	0.85	3.67	0.71	1.99	0.27	1.66	0.24	7.89	1.37
09SD-105	82.8	1240	19.8	188	4.45	13.8	0.72	2755	70.4	128.8	15.1	54.5	8.70	2.17	7.21	0.84	3.83	0.78	2.13	0.28	1.80	0.25	7.31	1.79
09SD-165	59.2	1562	26.3	319	6.80	19.3	1.09	1622	136.5	273.7	30.2	109.4	16.06	3.79	11.85	1.39	5.53	0.98	2.73	0.32	2.00	0.30	13.59	2.27
09SD-167	59.3	1503	25.4	309	6.39	19.0	1.10	1572	131.0	262.6	28.8	105.7	15.40	3.72	11.63	1.33	5.36	0.97	2.76	0.32	1.98	0.27	13.01	2.21
09SD-169	17.8	1521	26.1	312	6.64	19.2	1.12	1593	133.8	269.8	29.8	109.5	16.21	3.86	11.74	1.38	5.53	1.01	2.74	0.31	2.02	0.30	13.38	2.22
09SD-171	12.3	1256	22.5	242	5.21	14.3	0.77	1465	106.1	213.9	24.1	88.5	13.76	3.20	9.70	1.18	4.99	0.88	2.39	0.27	1.66	0.23	9.98	1.62
09SD-172	11.5	1234	22.3	241	5.18	14.4	0.76	1476	106.4	213.4	24.1	88.3	13.41	3.16	10.14	1.16	4.65	0.88	2.40	0.26	1.71	0.24	9.89	1.67
09SD-177	13.0	1220	23.3	253	5.38	14.9	0.85	1413	113.0	226.8	25.3	92.9	14.06	3.38	10.02	1.24	5.02	0.89	2.47	0.27	1.75	0.25	10.52	1.77
09SD-178	13.2	1482	25.9	313	6.76	18.8	1.00	1552	135.0	273.8	29.8	107.1	15.99	3.81	11.95	1.39	5.46	0.98	2.85	0.32	2.02	0.29	13.41	2.36
09SD-179	12.3	1194	22.7	243	5.39	14.4	0.77	1333	107.9	215.1	24.3	89.5	13.41	3.20	9.98	1.20	4.83	0.88	2.36	0.27	1.68	0.25	9.95	1.69
09SD-183	14.0	1225	23.7	253	5.44	15.1	0.97	1380	114.6	229.4	25.8	95.1	14.17	3.36	10.81	1.25	4.98	0.92	2.54	0.27	1.78	0.26	10.69	1.82
09SD-185	13.1	1243	23.9	257	5.54	15.2	0.88	1389	116.0	232.5	26.4	96.5	14.36	3.39	10.63	1.25	4.94	0.90	2.39	0.29	1.79	0.26	10.55	1.75

Sample	$^{87}Rb/^{86}Sr$	$^{87}Sr/^{86}Sr$	2σ	$^{87}Sr/^{86}Sr(i)$	$^{147}Sm/^{144}Nd$	$^{143}Nd/^{144}Nd$	2σ	$\varepsilon_{Nd}(t)$	$T_{DM}(Ma)$	$^{176}Lu/^{177}Hf$	$^{176}Hf/^{177}Hf$	2σ	$\varepsilon_{Hf}(t)$	$\Delta\varepsilon_{Hf}(t)$
09SD-106	3.4393	0.707784	7	0.70750	0.1089	0.512132	3	−8.6	1596	0.0111	0.282306	3	−14.8	−6.0
09SD-107	2.5354	0.707761	6	0.70749	0.1062	0.512126	3	−8.7	1561	0.0126	0.282318	2	−14.5	−5.6
09SD-108	2.7335	0.707816	5	0.70747	0.1056	0.512107	3	−9.0	1579	0.0102	0.282310	2	−14.6	−5.2
09SD-109	2.4441	0.707754	5	0.70747	0.1063	0.512130	3	−8.6	1558	0.0119	0.282307	3	−14.9	−6.0
09SD-110	4.5896	0.707770	7	0.70748	0.1062	0.512130	3	−8.6	1556	0.0104	0.282302	3	−14.9	−6.1
09SD-76	0.1250	0.712205	5	0.71192	0.0969	0.511646	3	−17.8	2055	0.0105	0.282288	2	−15.3	6.0
09SD-78	0.1246	0.710307	5	0.71003	0.1000	0.511639	4	−18.0	2122	0.0100	0.282286	3	−15.3	6.3
09SD-80	0.3084	0.709432	6	0.70921	0.0963	0.511696	3	−16.9	1980	0.0103	0.282361	2	−12.7	7.3
09SD-81	0.2960	0.709434	5	0.70921	0.0991	0.511688	3	−17.0	2041	0.0103	0.282357	3	−12.9	7.4
09SD-82	0.2895	0.709432	6	0.70920	0.0966	0.511684	3	−17.1	2000	0.0104	0.282354	3	−13.0	7.3
09SD-84	0.2712	0.709375	6	0.70916	0.0976	0.511691	3	−17.0	2009	0.0101	0.282363	3	−12.6	7.5
09SD-85	0.2808	0.709426	5	0.70921	0.0973	0.511692	4	−16.9	2003	0.0098	0.282358	3	−12.8	7.4
09SD-86	0.2861	0.709420	7	0.70921	0.0971	0.511688	3	−17.0	2005	0.0102	0.282371	3	−12.4	7.9
09SD-90	0.3202	0.709571	5	0.70922	0.1037	0.511674	3	−17.4	2150	0.0072	0.282278	3	−15.4	5.3
09SD-91	0.2510	0.709584	5	0.70932	0.0987	0.511660	3	−17.6	2071	0.0087	0.282258	2	−16.3	4.8
09SD-94	0.2583	0.709580	6	0.70929	0.1019	0.511654	3	−17.7	2140	0.0086	0.282256	2	−16.3	4.9
09SD-96	0.3289	0.709843	5	0.70956	0.0970	0.511655	3	−17.7	2046	0.0089	0.282251	2	−16.5	4.6
09SD-98	0.2746	0.708632	6	0.70846	0.0993	0.511666	3	−17.5	2074	0.0075	0.282205	2	−18.0	2.9
09SD-103	0.1827	0.709512	7	0.70920	0.0926	0.511660	3	−17.5	1960	0.0077	0.282196	2	−18.3	2.5
09SD-105	0.2261	0.709403	6	0.70907	0.0966	0.511663	4	−17.5	2027	0.0077	0.282195	3	−18.4	2.5
09SD-165	0.1096	0.709679	7	0.70948	0.0887	0.511882	3	−13.0	1632	0.0061	0.282277	3	−15.3	−0.4
09SD-167	0.1142	0.709650	5	0.70945	0.0881	0.511883	4	−13.0	1622	0.0059	0.282267	3	−15.6	−0.8
09SD-169	0.0339	0.709555	6	0.70949	0.0895	0.511925	3	−12.2	1590	0.0062	0.282268	2	−15.6	−1.9
09SD-171	0.0285	0.709736	5	0.70969	0.0940	0.511848	3	−13.8	1753	0.0063	0.282242	3	−16.5	−0.6
09SD-172	0.0270	0.709747	5	0.70970	0.0918	0.511843	3	−13.8	1723	0.0065	0.282236	3	−16.7	−0.8
09SD-177	0.0307	0.709796	5	0.70974	0.0915	0.511828	4	−14.1	1738	0.0064	0.282234	3	−16.8	−0.5
09SD-178	0.0258	0.709566	5	0.70952	0.0902	0.511876	4	−13.2	1659	0.0059	0.282270	3	−15.5	−0.5
09SD-179	0.0298	0.709748	6	0.70970	0.0905	0.511832	4	−14.0	1719	0.0064	0.282251	2	−16.2	0.0
09SD-183	0.0331	0.709788	4	0.70973	0.0900	0.511830	3	−14.1	1714	0.0066	0.282248	3	−16.3	−0.1
09SD-185	0.0306	0.709828	6	0.70977	0.0899	0.511833	3	−14.0	1708	0.0066	0.282245	3	−16.5	−0.3

Note: data for Fangcheng basalts are from Guo et al. (2013b). Other samples were analyzed in this study. $\Delta\varepsilon_{Hf}(t) = \varepsilon_{Hf}(t) - 1.36\varepsilon_{Nd}(t) - 2.89$.

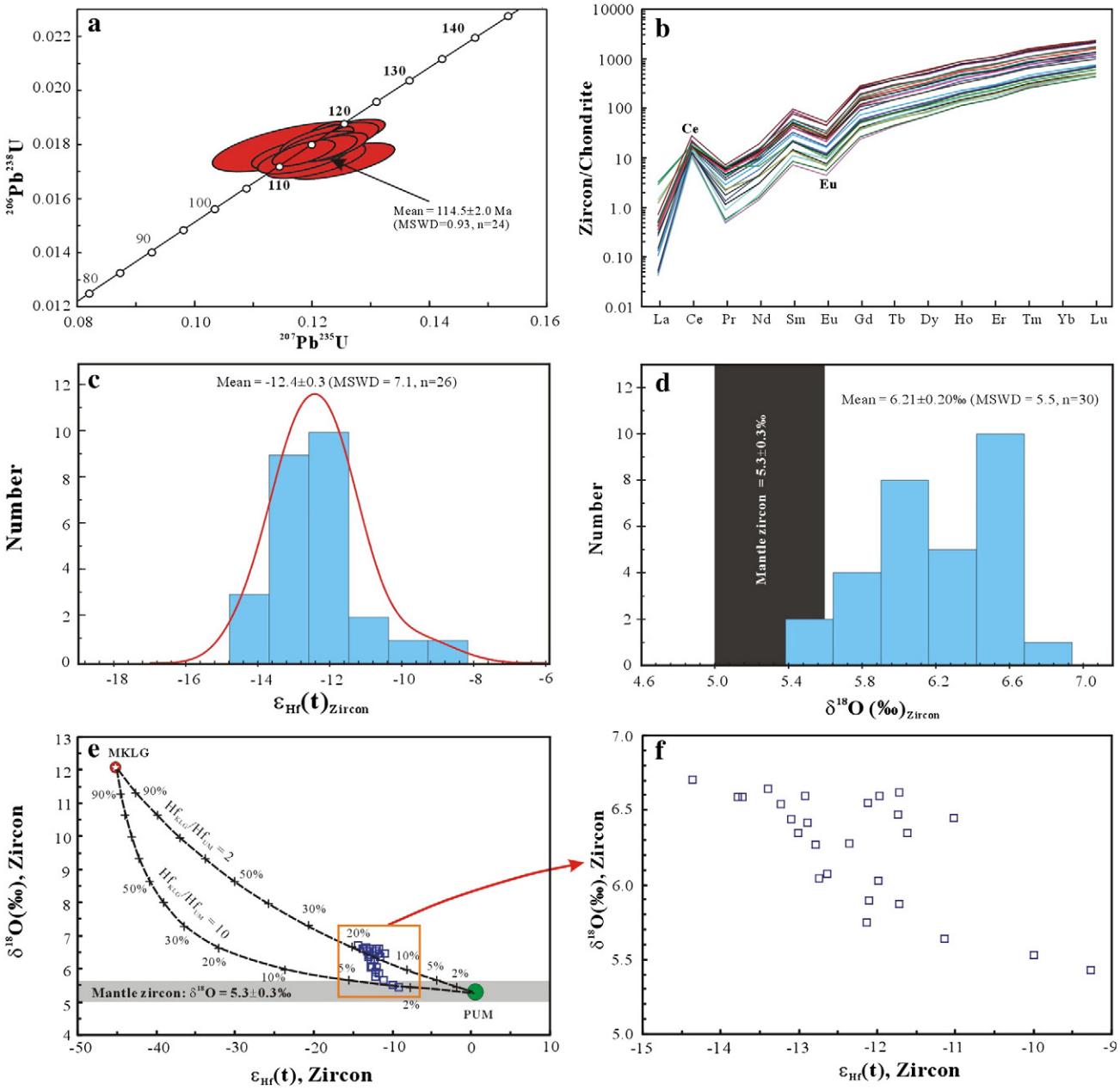

Fig. 2. (a) U–Pb zircon results, (b) chondrite-normalized REE patterns, (c) $\varepsilon_{Hf}(t)$ and (d) $\delta^{18}O$ isotopic histograms, (e) and (f) $\varepsilon_{Hf}(t)$ via $\delta^{18}O$ diagrams of zircons from the Rushan dioritic intrusion. Note that the $\varepsilon_{Hf}(t)$ of the Paleozoic upper mantle (PUM) of NCC is assumed to be in accordance with Hf isotopic compositions of perovskite in the Paleozoic kimberlites (Yang et al., 2009) and the $\delta^{18}O$ is assumed to be 5.3‰. The $\varepsilon_{Hf}(t)$ of the metasediments in the Kongling Group (MKLG) is recalculated in accordance with the zircon Hf isotopic compositions and whole-rock Lu/Hf ratios and the $\delta^{18}O$ is assumed to be 12‰. (Zhang et al., 2006; Gao et al., 1999).

give $\varepsilon_{Hf}(t)$ ranging between −14.4 and −9.3 with a mean $\varepsilon_{Hf}(t)$ of −12.4 ± 0.3 (MSWD = 7.1, n = 26, Fig. 2c). The zircons have $\delta^{18}O$ ranging from 5.4 to 6.7‰ with a mean $\delta^{18}O$ of 6.21 ± 0.20‰ (Fig. 2d), higher than that of mantle zircon ($\delta^{18}O$ = 5.3 ± 0.3‰, Valley, 2003). The estimated whole-rock $\delta^{18}O$ is roughly 7.2‰, similar to that estimated from olivine of the Fangcheng basalts and pyroxenites (Guo et al., 2013b; Xu et al., 2013). The zircons show a negative correlation between $\delta^{18}O$ and $\varepsilon_{Hf}(t)$ (Fig. 2e, f), indicating a mixing trend between mantle material and a non-radiogenic crustal component.

4.2. Whole-rock geochemistry

The Rushan diorite has a narrow compositional range (e.g., SiO_2 = 56.8–57.1 wt.%). MgO (3.3–3.4 wt.%) and Mg# (~46) are rather low compared with mantle-derived primary magmas, with correspondingly low Cr (46–88 ppm) and Ni (11–21 ppm), and high concentrations of strongly incompatible trace elements (e.g., Rb = 64–77.4 ppm, Th = 8.5–10.8 ppm, Zr = 116–157 ppm). K_2O/Na_2O ratios are < 1, Al_2O_3 (>17.5 wt.%), Sr (1042–1111 ppm) and Ba (1692–1819 ppm) concentrations are high, as are Sr/Y (48–54) ratios (Table 2). In comparison, the earlier (120–130 Ma) mafic dykes of the Sulu Orogen and the Fangcheng basalts have lower SiO_2, higher MgO (up to 11.9 wt.%) and significantly higher Mg# (typically between 65 and 73) with correspondingly higher Cr and Ni. The Rushan diorites and the mafic dykes show overlapping concentration ranges for most incompatible trace elements (e.g., LREE, Th), while the high-MgO Fangcheng basalts show highly enriched concentrations of these elements (Fig. 3a, b). There are broad trends

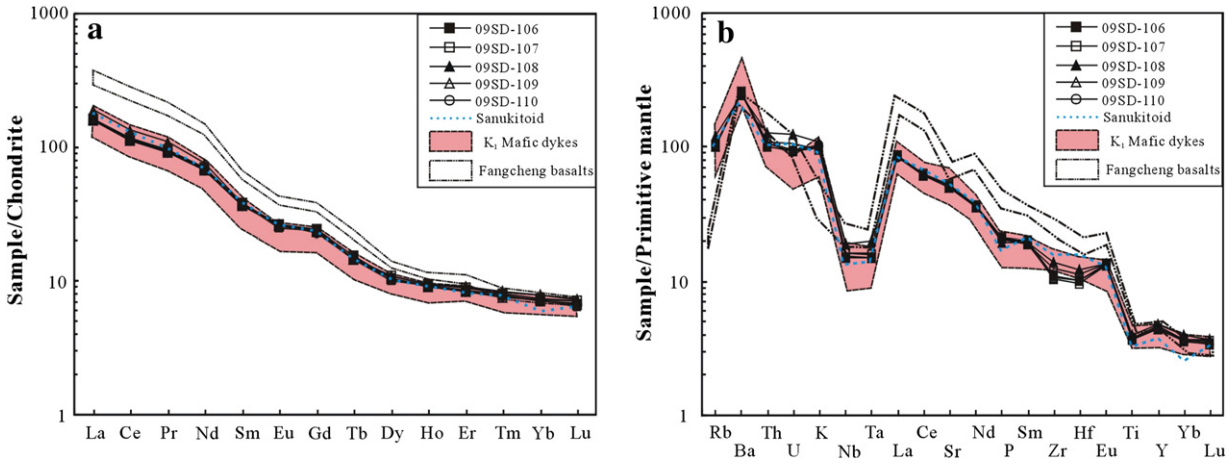

Fig. 3. (a) Chondrite-normalized REE patterns and (b) primitive mantle-normalized trace element patterns of the Rushan diorite samples, the mafic dykes and Fangcheng basalts. Data sources: Rushan diorite and mafic dykes — (this study); Fangcheng basalts — Guo et al. (2013b); average sanukitoid — Martin et al. (2005); chondrite — Taylor and McLennan (1985); primitive mantle — Sun and McDonough (1989).

of increasing Mg#, Cr, Ni, Zr and La/Nb from the diorite to mafic dykes to the Fangcheng basalts (Fig. 4a–d).

Compared to the mafic dykes and Fangcheng basalts, the Rushan diorites have similar whole-rock Hf isotopic compositions ($\varepsilon_{Hf}(t) = -14.9$ to -14.5) but less radiogenic Sr and more radiogenic Nd isotopic compositions (Table 2). All the studied rocks show a Sr–Nd isotopic variation trend to EMII (Fig. 5a). The diorites plot below the terrestrial array in $\varepsilon_{Nd}(t)$–$\varepsilon_{Hf}(t)$ isotope space (Fig. 5b) having less radiogenic Hf than Nd, with $\Delta\varepsilon_{Hf}(t)$ ($\Delta\varepsilon_{Hf}(t) = \varepsilon_{Hf}(t) - 1.36 \times \varepsilon_{Nd}(t) - 2.89$, Vervoort et al., 1999) ranging between −6.1 and −5.2. In this respect they contrast with the earlier Fangcheng basalts which lie on or close to the terrestrial array and with the mafic dykes that have positive $\Delta\varepsilon_{Hf}(t)$ between 2.5 and 7.9. The highly negative $\Delta\varepsilon_{Hf}(t)$ values of the Rushan diorites have been observed in zircon-bearing sediments such as recycled orogenic sandstones and marine turbidities (Richards et al., 2005; Vervoort et al., 2011).

The initial Sr isotopic compositions become more radiogenic from the diorite to mafic dykes to the Fangcheng basalts and this trend broadly correlates with increasing Cr, and Ni concentrations, and Mg# (Fig. 6a, b, c), whereas the $\varepsilon_{Nd}(t)$ decreases from the diorite to Fangcheng basalts to the mafic dykes (Fig. 4d).

5. Discussion

5.1. Magmatic differentiation

The Rushan dioritic intrusion shares several compositional features with sanukitoids that are widely considered to form through melting of a mantle source metasomatically enriched by addition of slab-derived fluids or melts (Shirey and Hanson, 1984; Martin et al., 2005; Guo et al., 2007). These features include Al_2O_3-rich compositions with high LILE concentrations and high Sr/Y ratios (Table 2). Like sanukitoids, the diorites also show LILE and LREE enrichments, small negative Eu anomalies (Fig. 4a), and Nb–Ta–Zr–Hf–Ti depletions in primitive mantle-normalized trace element diagrams (Fig. 4b). Unlike sanukitoids, however, the diorites have Mg# that are too low (~46) to reflect equilibration with the mantle (c.f. >60), and this is supported by correspondingly low concentrations of Cr and Ni. These compositional ranges, accompanied by rather high concentrations of Th and LREE likely reflect moderate degrees of fractionation.

Nevertheless, the Rushan dioritic intrusion has MgO or Mg# higher than expected for melts derived from metabasalts (e.g., MgO <3 wt.% and Mg# <45, Rapp and Watson, 1995) and so their parental melts are most likely of mantle origin. Compared with the earlier mafic rocks, the Rushan diorite has more radiogenic Nd and less radiogenic Sr isotopic compositions (Fig. 3c), arguing against an origin by differentiation of the earlier mafic dykes or the Fangcheng basalts, and against a genetic link through crustal contamination or assimilation–fractional crystallization (AFC) processes (Fig. 6). When compared with the NCC lithospheric mantle, the Rushan dioritic intrusion has less radiogenic Nd and Hf, and more radiogenic Sr isotopic compositions as well as higher $\delta^{18}O$ values, requiring an additional crustal component with highly evolved Sr–Nd–Hf–O isotopic compositions in the mantle source (Figs. 2e and 5). This "crustal" component is even more apparent in the high-Mg# mafic dykes and the Fangcheng basalts, which clearly do have major element compositions that reflect mantle derivation. These two basalt types cannot be related to each other by fractional crystallization, as evidenced from the relationships of Zr and $\varepsilon_{Nd}(t)$ with Mg# (Fig. 4c and 6d). Furthermore, the observation that Mg#, Ni and Cr show no correlation with $^{87}Sr/^{86}Sr(i)$ for both the dyke and basalt samples suggests that the enriched isotopic and trace element compositions are not the result of crustal contamination or AFC during magma emplacement (Fig. 6a–c). These compositional features reflect a mantle source enriched by a "crustal" component.

In the Sulu Orogen and its adjacent regions, exposed Archean to Proterozoic metamorphic complexes, e.g., such as those occurring at Haizhou, Wulian, Penglai, Fenzishan and Jingshan (Zhou et al., 2008a,b, c, 2012) could provide a source of crustal components. Recycling of these crustal materials into the mantle would require lithospheric delamination. However, a delamination model is not supported by the geological record. Delamination of a thickened lithosphere would lead to rapid uplift of the Sulu Orogen (Menzies et al., 2007), but evidence is lacking for such uplift during the Early Cretaceous. Lithospheric delamination would induce asthenospheric upwelling, leading to decompression melting and formation of basalts with similar geochemical features to MORBs or OIBs. The absence of such asthenospheric magmas contemporaneous with the Rushan diorite thus argues against the delamination of the lithospheric mantle and eclogitic crust. Furthermore, the lower mafic crust is characterized by relatively low $\delta^{18}O$ (i.e. <7‰). Addition of bulk lower mafic crust or their melts cannot account for the high $\delta^{18}O$ (around 7.2‰) of the Rushan dioritic intrusion and the Fangcheng basalts.

Another candidate for the recycled crustal component may be the subducted sediment from the paleo-Pacific Plate. In accordance with the geophysical observations (e.g., Engebretson et al., 1985), oblique subduction of the Izanagi Plate toward the NCC occurred during the

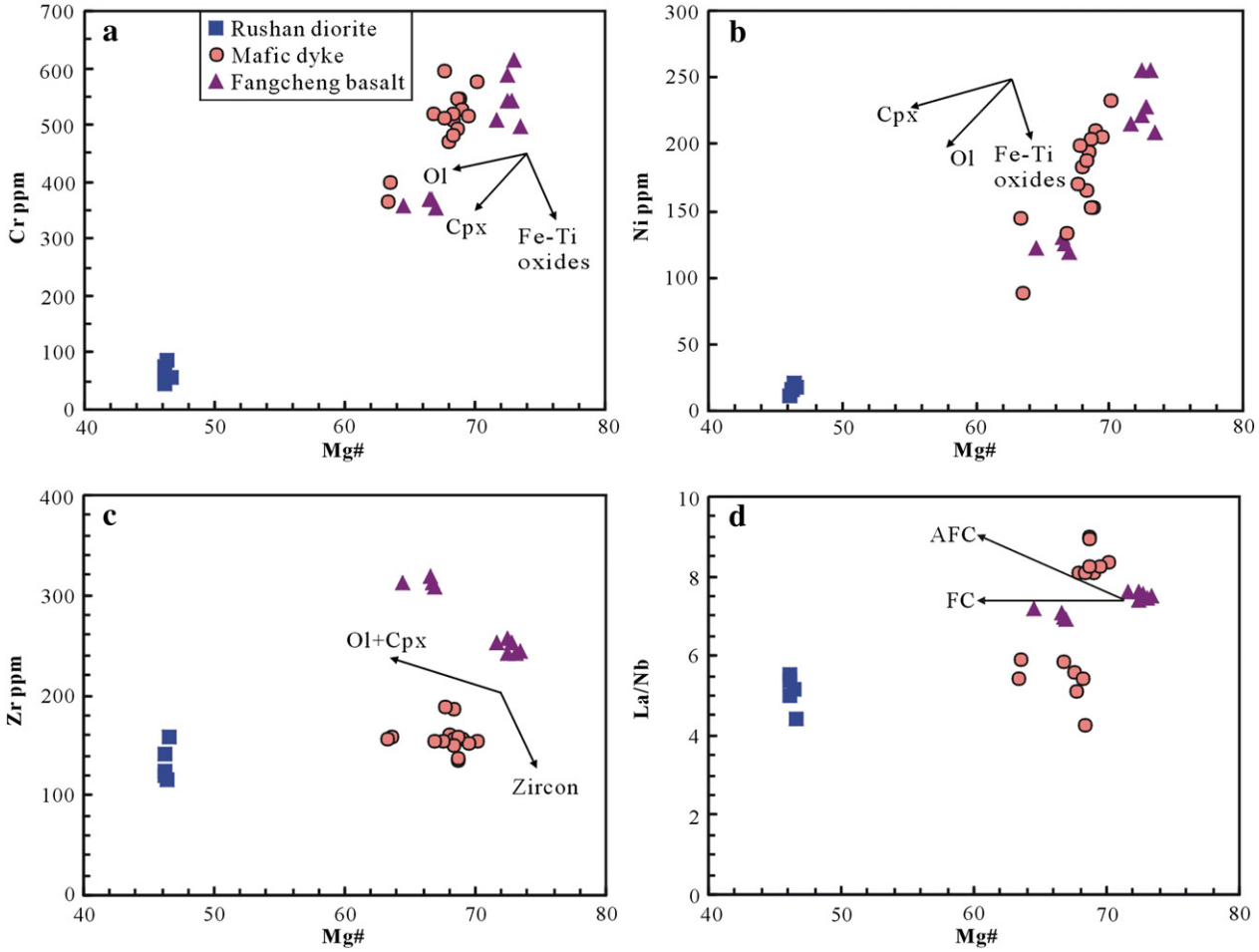

Fig. 4. Mg# versus Cr (a), Ni (b), Zr (c) and La/Nb (d) plots of the Rushan diorite, mafic dykes and Fangcheng basalts, showing the possible role of fractional crystallization (FC) and assimilation–fractional crystallization (AFC) during magmatic evolution. Note that the Rushan diorite has relatively lower concentrations of Cr, Ni and Zr and La/Nb ratio than those of mafic rocks. Cr mineral abbreviations: Ol — olivine; Cpx — clinopyroxene.

Early Cretaceous, which was a likely driving force for the large-scale magmatism and crustal deformation in eastern China (Wu et al., 2005). However, marine sediments generally have positive $\Delta\varepsilon_{Hf}$ values due to the "zircon effect" — loss of zircon during transportation and deposition (e.g., Vervoort et al., 2011). The incorporation of subducted marine sediments from the paleo-Pacific Plate cannot explain the negative $\Delta\varepsilon_{Hf}(t)$ observed in the Rushan diorite.

By contrast with the exposed Archean–Proterozoic metamorphic complexes and the marine sediments, we suggest that the most likely candidates for the required crustal components are the continental sediments from the Yangtze Block, which had been subducted beneath the NCC during the Triassic. For instance, the metasediments of the Kongling Group (MKLG) from the Yangtze Block, which have the required compositional characteristics including high $\delta^{18}O$ (the quartz has $\delta^{18}O$ values of about 11‰), very unradiogenic Nd–Hf isotopic compositions and high Th and U concentrations (Gao et al., 1999; Zhang et al., 2006).

Moreover, some compositional trends between the three groups of igneous rocks, in particular trends to higher initial Sr-isotopic ratios with increasing Cr and Ni concentrations and increasing Mg# (Table 2; Fig. 6a–c), suggest that the degree of mantle enrichment was in fact influenced by the amount of crustal material initially introduced into the source, either as fluids/melts reacting with the surrounding mantle to form metasomatic veins or pyroxenites, or as sedimentary restites physically retained within the lithospheric mantle. Thus, the suggestion here is that flux-melting may play a role in the production of some mantle-derived melts during the Triassic subduction of the Yangtze continental sediments.

5.2. Enrichment processes in the lithospheric mantle

A striking feature of the Early Cretaceous Rushan dioritic intrusion is the highly negative $\Delta\varepsilon_{Hf}(t)$ values, which have rarely been observed in modern arc magmas. Numerous studies have shown that marine turbidities, zircon-bearing sands and recycled orogenic sandstones contain less radiogenic Hf than Nd due to the "zircon effect" on the Lu–Hf and Sm–Nd isotope systems (e.g., Vervoort et al., 1999, 2011; Richards et al., 2005; Carpentier et al., 2009). Available data for the MKLG from the Yangtze Block indicate that they also have highly nonradiogenic Nd–Hf isotopic compositions with less radiogenic Hf than Nd (Gao et al., 1999; Zhang et al., 2006) as do some Neoproterozoic low-grade metasedimentary rocks from the Yangtze Block (Wang et al., 2010). This decoupling strongly supports the suggestion that these sedimentary components of the Yangtze continental crust are the source of mantle enrichment beneath the region, but this does not immediately explain the large range of $\Delta\varepsilon_{Hf}(t)$ values shown by the three groups of rocks.

The metasomatic introduction of a subducted sediment component into a mantle source can be either fluid- or melt-mediated (e.g., Macdonald et al., 2000; Hanyu et al., 2006). In the case of aqueous fluid-mediated enrichment, Nd is much more mobile than Hf (e.g., You et al., 1996; Kessel et al., 2005), and so the mantle wedge is likely to inherit the typically unradiogenic Nd of subducted

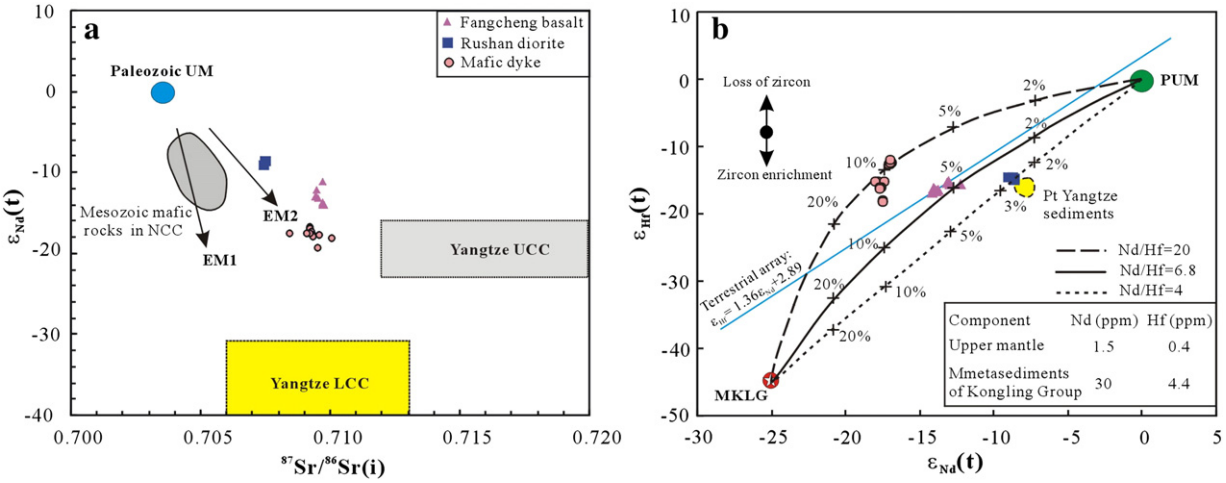

Fig. 5. (a) Sr–Nd isotope diagram of Rushan diorite, mafic dykes and Fangcheng basalts, showing an EMII-like Sr–Nd isotopic character. (b) Hf–Nd isotope diagram, showing the results of source mixing between subducted sediments represented by MKLG and PUM of NCC. Note that the varied Nd/Hf ratios during modeling represent the addition of different melts or restite from the subducted MKLG to the mantle source. The curve with Nd/Hf = 4 shows the mixing result between the metasedimentary restite and PUM, the curve with Nd/Hf = 20 shows the mixing result between the 'cold' low-degree (F = 0.1) sediment melt and PUM, and the curve with Nd/Hf = 6.8 shows the mixing result between the 'hot' high-degree (F = 0.3) sediment melt and PUM.
Data sources: PUM — Yang et al. (2009); Mesozoic mafic rocks in NCC — Guo et al. (2001, 2013a); Yangtze LCC and UCC — Gao et al. (1999); Hf–Nd terrestrial array — Vervoort et al. (1999); Nd–Hf–O isotopic compositions of MKLG — Gao et al. (1999) and Zhang et al. (2006); Pt Yangtze sediments — Neoproterozoic metasediments of the Lengjiaxi and Banxi Groups from the Yangtze Block (Wang et al., 2010).

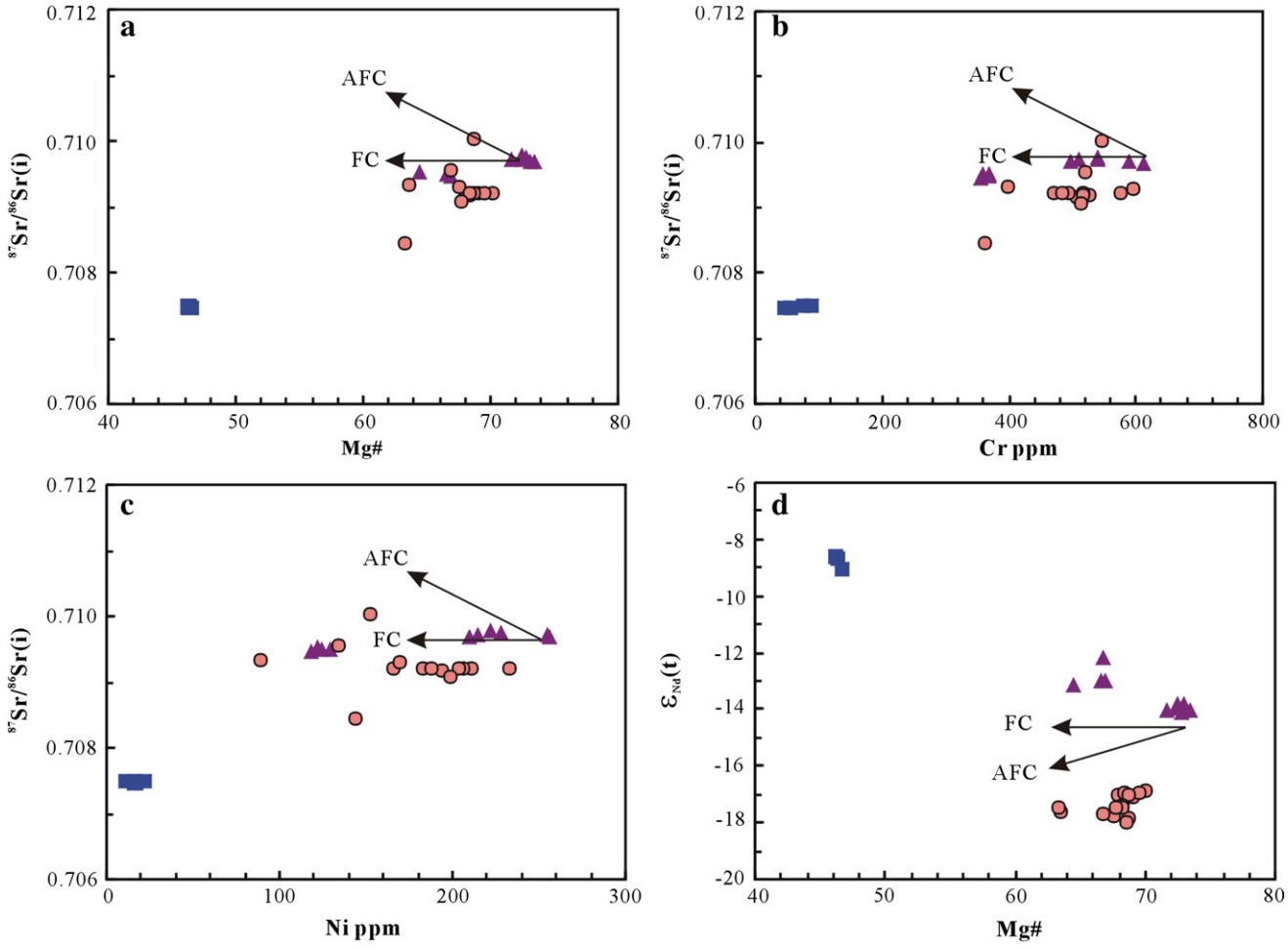

Fig. 6. Mg# (a), Cr (b) and Ni (c) versus $^{87}Sr/^{86}Sr(i)$ and Mg# versus $\varepsilon_{Nd}(t)$ (d) plots of the Rushan dioritic intrusion and related mafic rocks in the southwestern NCC. Note that the Rushan dioritic intrusion cannot be produced through FC or AFC processes of the more primitive mafic dykes or the Fangcheng basalts. Also, there is a lack of variation trends of FC or AFC processes between the mafic dykes and the Fangcheng basalts. Rather, the difference in initial Sr isotopic composition among these three rock types was attributed to the source variation enriched via the subduction of the Yangtze sediments.

Table 3
Trace elemental modeling parameters and results of Rushan diorite and mafic magmas in the southeastern NCC.

Element	Rb	Ba	Th	U	K	Nb	Ta	La	Ce	Sr	Nd	Sm	Zr	Hf	Eu	Y	Yb	Nd/Hf
PUM	0.65	20	0.1	0.025	0.06	0.8	0.05	1.2	2.5	30	1.5	0.6	15	0.4	0.2	4.5	0.48	3.8
MKLG	130	600	9	2.5	3	13	0.90	36	70	165	30	5.5	180	4.4	1.2	30	3	6.8
K_D ('cold' melting)	0.15	0.2	0.2	0.2	0.15	0.15	0.15	0.15	0.15	0.2	0.1	0.2	0.5	0.5	0.2	1.5	1.5	0.2
F = 0.1	553	2143	32.1	8.9	12.8	55.3	3.83	153	298	589	158	19.6	327	8.0	4.3	20.7	2.1	19.7
Restites	83.0	429	6.4	1.8	1.9	8.3	0.57	23.0	44.7	117.9	15.8	3.9	164	4.0	0.9	31.0	3.1	3.9
K_D ('hot' melting)	0.15	0.2	0.2	0.2	0.15	0.15	0.15	0.15	0.15	0.2	0.2	0.2	0.2	0.2	0.2	1.5	1.5	1.0
F = 0.3	321	1364	20.5	5.7	7.4	32.1	2.22	88.9	173	375	68.2	12.5	409.1	10.0	2.7	22.2	2.2	6.8
Restites	48.1	272.7	4.09	1.1	1.1	4.8	0.33	13.3	25.9	75.0	13.6	2.5	81.8	2.0	0.5	33.3	3.3	6.8
Rushan dioritic intrusion (~115 Ma)																		
Source (MKLG rest. = 0.03)	3.12	32.3	0.29	0.08	0.12	1.02	0.07	1.85	3.77	32.6	1.93	0.70	19.5	0.51	0.22	5.30	0.56	3.8
Bulk K_D	0.03	0.001	0.012	0.015	0.02	0.08	0.08	0.015	0.015	0.01	0.02	0.06	0.12	0.12	0.08	0.25	0.3	0.17
Melting degree (F = 0.02)	63.2	1538	9.1	2.2	2.9	10.4	0.7	53.4	109	1095	48.7	8.9	141	3.7	2.2	20.0	1.8	13.2
Average (n = 5)	67.6	1765	9.3	2.1	3.0	11.7	0.7	59.1	110	1076	48.8	8.6	132	3.3	2.3	20.8	1.8	14.8
Mafic dykes (120–130 Ma)																		
Source (MKLG melt = 0.1, F = 0.1)	55.9	232.3	3.30	0.92	1.33	6.25	0.43	16.4	32.0	85.9	17.1	2.50	46.2	1.16	0.61	6.12	0.64	14.8
Bulk K_D	1.1	0.01	0.35	0.5	0.5	0.6	0.6	0.15	0.15	0.001	0.2	0.2	0.2	0.2	0.2	0.25	0.3	1.0
Melting degree (F = 0.1)	51.3	2131	7.96	1.66	2.42	9.77	0.67	69.8	136	852	61.2	8.94	165	4.14	2.17	18.8	1.73	14.8
Average (n = 13, MgO > 8%)	53.1	2148	8.56	1.46	2.46	9.34	0.57	64.7	120	980	50.9	8.22	157	3.76	2.06	18.3	1.73	13.6
Fangcheng basalts (~125 Ma)																		
Source (MKLG melt = 0.05, F = 0.3)	16.6	86.2	1.11	0.31	0.42	2.32	0.16	5.52	10.9	45.8	4.76	1.17	34.0	0.86	0.32	5.16	0.54	5.5
Bulk K_D	1.20	0.02	0.07	0.15	0.45	0.12	0.15	0.01	0.01	0.001	0.01	0.05	0.10	0.12	0.05	0.2	0.3	0.08
Melting degree (F = 0.04)	14.0	1456	10.4	1.67	0.90	14.98	0.85	111	220	1117	95.9	13.2	250	5.54	3.60	22.2	1.66	17.3
Average (n = 6, MgO > 11%)	12.7	1409	10.3	1.72	0.93	14.73	0.83	111	222	1229	91.8	13.9	248	5.36	3.28	23.1	1.73	17.1

PUM — assumed Paleozoic upper mantle of NCC; MKLG — average compositions of the metasediments of Kongling Group from the Yangtze Block (Gao et al., 1999).
The residual assemblage for sediment melting is assumed to be garnet + pyroxene + K-rich mineral (e.g., phengite) + Al-rich mineral (e.g., zoisite and allanite) with little or no plagioclase (Hermann and Spandler, 2008). The terms of "cold" and "hot" melting represent low-degree and high-degree melting of the subducted sediments with residual zircon and no zircon, respectively. The bulk distribution coefficient (K_D) values for mantle melting are estimated based on a residual assemblage of olivine + pyroxene + garnet ± phlogopite. Residual garnet is evident to account for strong LREE/HREE fractionation in these three suites. Hydrous melting with residual phlogopite is supposed to account for the high bulk K_D values of Rb and K for the mafic dykes and Fangcheng basalts (Xia et al., 2013; Guo et al., 2013b). MKLG rest. = 0.03 — the proportion of restite of MKLG left by cold melting (F = 0.1) was 0.03; MKLG melt = 0.1, F = 0.1 — the proportion of melt derived from MKLG by cold melting (F = 0.1) was 0.1; MKLG melt = 0.05, F = 0.3 — the proportion of melt derived from MKLG by hot melting (F = 0.3) was 0.05.

sediments but retain mantle Hf isotopic compositions — i.e., the mantle wedge will acquire less radiogenic Nd than Hf, and positive $\Delta\varepsilon_{Hf}(t)$ values, as is observed in most arc basalts (e.g., Jicha et al., 2004).

In the case of subducted sediment-derived melts, the degree of Hf–Nd isotopic decoupling is mainly dependent on the melting temperature and on the isotopic composition of the subducted sediments themselves (Nichols et al., 1994; Tollstrup and Gill, 2005; Nebel et al., 2011). During "hot-subduction" (i.e. T >830 °C, Johnson and Plank, 1999), high-degree partial melting of sediments leaves little or no residual zircon, and the melt-metasomatized mantle will directly acquire the $\Delta\varepsilon_{Hf}(t)$ value of the subducted sediments. Thus, subduction of pelagic zircon-poor sediments with typically positive $\Delta\varepsilon_{Hf}(t)$ values, and subduction of terrestrial zircon-rich sandstones and recycled orogenic sandstones, with negative $\Delta\varepsilon_{Hf}(t)$ values, will impart these characteristics on to the mantle. During cold subduction (i.e. T <780 °C, Tollstrup and Gill, 2005; Nakamura and Iwamori, 2013), perhaps more applicable to continental subduction, zircon may be variably residual during melting of sediments. If zircon is largely residual, the melt-modified mantle wedge could acquire positive $\Delta\varepsilon_{Hf}(t)$ values, even if the subducted sediment had negative $\Delta\varepsilon_{Hf}(t)$ values (Fig. 5b).

We suggest that the positive $\Delta\varepsilon_{Hf}(t)$ values of the mafic dykes of the Sulu Orogen were probably derived in this way — through "cold" subduction of Yangtze lithosphere. The 'cold' sediment melt, which is characterized by high Nd/Hf ratio with less radiogenic Nd and more radiogenic Hf, reacts with the surrounding mantle peridotite to form the metasomatic vein. In contrast, the metasedimentary zircon-bearing restites, after removal of the "cold" melt, will have low Nd/Hf ratio with more radiogenic Nd and less radiogenic Hf, and we suggest that physical incorporation of this residue into the mantle provided the highly negative $\Delta\varepsilon_{Hf}(t)$ source for the dioritic intrusion.

The interaction of sediment melts with the overlying mantle will form fertile mantle pyroxenite. Partial melting of this fertile, olivine-poor, pyroxenite will produce Mg-rich magmas with high Ni-concentrations. It has indeed been suggested that fertile pyroxenites formed through sediment melt–peridotite interaction were the source of the high-MgO basalts from Fangcheng and Feixian (Zhang et al., 2002; Gao et al., 2008; Guo et al., 2013b). The Rushan dioritic intrusion, which has low MgO (also Cr and Ni) Mg# and $^{87}Sr/^{86}Sr(i)$ and an andesitic composition, could not be produced through direct melting of the same source as the Fangcheng basalts.

Based on the above discussion, the origin of the Rushan diorite is attributed to melting of a lithospheric mantle containing highly negative $\Delta\varepsilon_{Hf}(t)$ zircon-bearing metasedimentary restites of the MKLG, which had been previously melted to variable degrees during the subduction of the Yangtze lithosphere in a continental subduction channel (Zheng, 2012). The sedimentary restites were preserved in the lithospheric mantle, which took on a pudding-cake compositional structure. The conjugate "cold" MKLG sediment melts interacted with the overlying mantle to form the source for the mafic dykes (positive $\Delta\varepsilon_{Hf}(t)$ values) in the Sulu Orogen, whereas interaction between the "hot" sediment melts, with little or no residual zircon, and upper mantle possibly formed the source of the high-MgO Fangcheng and Feixian basalts ($\Delta\varepsilon_{Hf}(t) = -1.9 \sim 0$).

In order to test this model, we carried out numerical geochemical modeling. To simplify the modeling, we assumed that the Paleozoic

upper mantle (PUM) of the NCC had: Nd = 1.5 ppm, Hf = 0.4 ppm, $\delta^{18}O$ = 5.5‰, $\varepsilon_{Nd}(t) = 0$ and $\varepsilon_{Hf}(t) = 0$ based on the Nd and Hf isotopic compositions of perovskite within the Mengyin kimberlites (Yang et al., 2009). The MKLG has: Nd = 30 ppm, Hf = 4.4 ppm, $\delta^{18}O$ = 12‰, $\varepsilon_{Nd}(t) = -25$ and $\varepsilon_{Hf}(t) = -45$ based on the average geochemical data compiled from Gao et al. (1999) and Zhang et al. (2006). The trace element compositions of the end-member components and calculation conditions are listed in Table 3.

The modeling results indicate that the addition of ~3% restite with Nd/Hf = 4 from the MKLG into the PUM could produce the observed Hf–Nd isotopic compositions, and 2% melting of this mixed source could create the average trace element compositions of the Rushan diorite (Fig. 4b and 7a). Addition of ~10% MKLG melt (F = 0.1) with Nd/Hf = 20 into the PUM and 10% melting of the mixed source could form the Hf–Nd isotopic compositions and the average compositions of the Early Cretaceous mafic dykes (Fig. 4b and 7b). Addition of ~5% MKLG melt (F = 0.3) with Nd/Hf = 6.8 into the PUM and 4% melting of that mixed source could produce the Hf–Nd isotopic compositions and the average chemical composition of the Fangcheng basalts (Fig. 4b and 7c).

5.3. Implications for crustal recycling in a continental subduction setting

Compared to oceanic slabs, subducting continental lithosphere is relatively cool with low water content. This is why there is a lack of syn-subduction magmatism in the Dabie–Sulu orogenic belt. The "cold" melt derived from the subducted fertile sediments would migrate and interact with the surrounding mantle to form metasomatic veins within the subduction channel (Guo et al., 2004; Zheng, 2012). Such metasomatic veins were an important source component for the Early Cretaceous calc-alkaline lamprophyres in the Sulu Orogen (Guo et al., 2004). They were likely the source for the Late Triassic syenites (Zhao et al., 2012) that simultaneously formed during the exhumation of UHP rocks in response to slab breakoff. Detachment of the subducted continental slab led to heating and subsequent high-degree melting of the subducted sediments. The resulting melts interacted with the mantle to form the pyroxenites, which were the melting sources for the later high-MgO Fangcheng and Feixian basalts (Zhang et al., 2002; Gao et al., 2008; Guo et al., 2013b). During the Early Cretaceous, oblique subduction of the paleo-Pacific Plate exerted a driving force to induce the extensive collapse of the southeastern margin of the NCC and trigger extensive melting of the metasomatized mantle to form the mafic magmas and the Rushan diorite.

Our new results indicate that although most of the subducted Yangtze lithosphere had been exhumed to crustal levels or detached into the convective asthenosphere, there probably existed a certain volume of subducted recycled sediments that served as a fertile component in the melting source for the Early Cretaceous magmas beneath the Sulu Orogen. Compared with the fertile sediments, the recycled sedimentary restites, which had experienced different degrees of melting, are chemically refractory and difficult to remelt. Also, these recycled crustal materials were probably trapped within the continental subduction channel to avoid thermal perturbation from the convective asthenosphere. The relatively 'cold' and thick lithosphere beneath the Sulu Orogen during Late Triassic to Jurassic was favorable for preservation of the sedimentary restites. The existence of recycled crustal components with high-$\delta^{18}O$ values over 100 million years (i.e., the time interval between the Early Triassic subduction of the Yangtze lithosphere and the Early Cretaceous large-scale mantle melting) requires that the 'crustal signatures' were retained within the cold and thickened lithosphere as metasomatic veins or lenses, forming a pudding-cake lithospheric structure beneath the orogen. Such a pudding-cake structure may exist beneath the mantle lithosphere of the Alpine–Himalaya orogen, in which the subducted continental crust-derived sediment is considered to have been stored within the subcontinental lithospheric mantle (Prelević et al., 2013). Thus subduction of chemically fertile sediments in a continental subduction zone can play an important role in crustal recycling processes and in producing compositional heterogeneity of subcontinental lithospheric mantle. It is therefore likely that such enrichment processes caused by subducted continental sediments are more important through geological time than previously thought (e.g., Zheng, 2012).

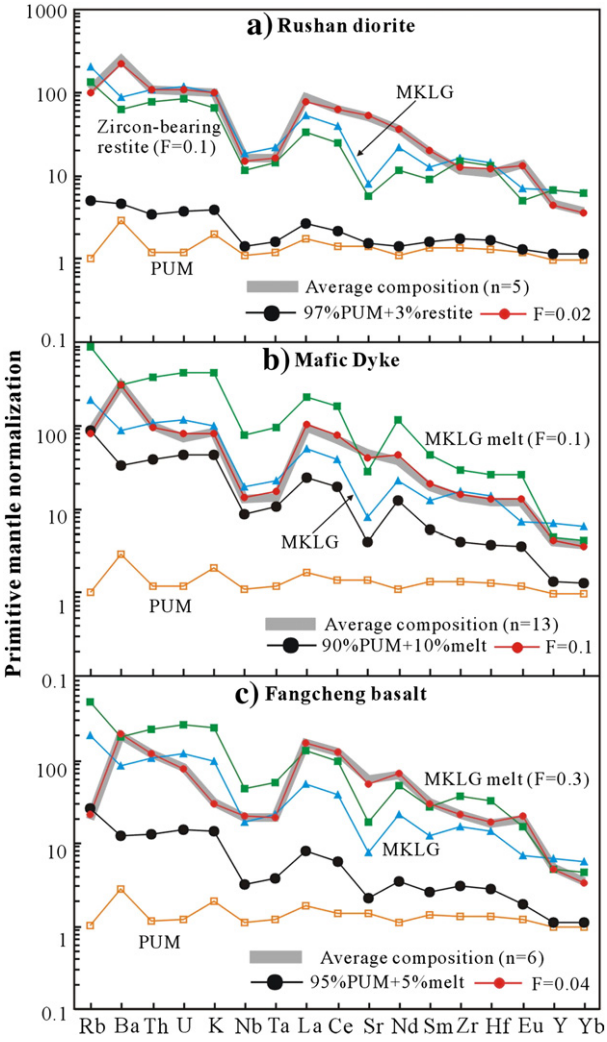

Fig. 7. Trace element modeling results of (a) the Rushan dioritic intrusion, (b) earlier mafic dykes and (c) high-MgO (>11 wt.%) Fangcheng basalts. During the trace element modeling, we used the modal melting equation to calculate the elemental concentrations of the melts and restites. Modeling parameters and results are listed in Table 3. The trace element compositions of the mixed sources (i.e., the mixing proportions between the PUM and the MKLG) are estimated from the Hf–Nd isotopic modeling results in Fig. 3d, in which the proportions of MKLG restite or melt are about 3%, 5% and 10% respectively, for the Rushan diorite, Fangcheng basalts and mafic dykes. The red line denotes the melt compositions derived from the mixed sources, e.g., F = 0.02 (Fig. 5a) points to the composition of the melt through 2% melting of the mixed mantle source with 97% PUM and 3% metasedimentary restite. The green line represents the composition of sediment melt or restite, e.g., MKLG melt (F = 0.3, Fig. 5c) points to the melt composition of the metasediments of the Kongling Group with melting degree of 30%. The blue line represents the composition of metasediments of the Kongling Group and the yellow line represents the composition of the assumed upper mantle of NCC.

6. Conclusions

The Early Cretaceous Rushan dioritic intrusion shows geochemical features similar to those of sanukitoids, with high concentrations of Al_2O_3, Sr, Ba, and $\delta^{18}O$, and Sr/Y ratios. The highly negative $\Delta\varepsilon_{Hf}(t)$ values of the diorites were probably derived from a restitic zircon-

bearing component of recycled sediment within the lithospheric mantle beneath the Sulu Orogen. The differing degrees of Hf–Nd isotopic decoupling among the diorites, the Fangcheng basalts and the mafic dykes were attributed to the different proportional involvement of the subducted Yangtze sediments or their melts, incorporated into the lithospheric mantle as metasomatic veins or restite lenses, forming a pudding-cake structure beneath the Sulu Orogen. Such a pudding-cake lithospheric structure may be prevalent beneath the collisional orogens involved in continental subduction.

Acknowledgments

We thank Y. Liu, L. Qi and Z.R. Ren for their help with whole-rock geochemical analyses, and J.H. Yang, X.H. Li and Y.H. Yang for *in situ* zircon U–Pb–Hf–O isotope and REE analyses. H.R. Smithies is thanked for checking the English language. Discussion with Y.F. Zheng helped improve the manuscript. We are grateful for constructive comments and suggestions by the Editor L. Reisberg, S. Wilde and an anonymous referee. This research was financially supported by the National Natural Science Foundation of China (90914009 and 41121002).

Appendix

Appended Table 1
The certified and analyzed values of international standards in major oxides analysis by XRF.

Sample	GSR-1 (granite)		GSR-2 (andesite)		GSR-3 (basalt)	
	This work n=4	reference	This work n=5	reference	This work N=8	reference
$S1O_2$	72.83±0.15	72.83	60.62±0.22	60.62	44.64±0.16	44.64
Al_2O_3	13.40±0.11	13.40	16.17±0.18	16.17	13.83±0.2	13.83
TFe_2O_3	2.14±0.08	2.14	4.90±0.09	4.90	13.4±0.29	13.40
FeO	1.03		2.43		7.60	
MgO	0.42±0.05	0.42	1.72±0.08	1.72	7.77±0.26	7.77
CaO	1.55±0.07	1.55	5.20±0.11	5.20	8.81±0.14	8.81
Na_2O	3.13±0.09	3.13	3.86±0.11	3.86	3.38±0.07	3.38
K_2O	5.01 ±0.10	5.01	1.89±0.07	1.89	2.32±0.08	2.32
TiO_2	0.172±0.01	0.29	0.309±0.014	0.52	1.42±0.061	2.36
MnO (ppm)	598±27	0.06	780±27	0.08	1691±94	
P_2O_5 (ppm)	928±30	0.093	2360±37	0.24	9462±85	0.95
LOI (900°C)	0.76±0.06	0.69	4.60±0.20	4.44	2.25±0.10	2.24
Total	99.783	99.613	99.80	99.64	99.88	99.87

Appended Table 2
The certified and analyzed values of international standards in trace elements analysis by ICP-MS.

Element	Concentration (ppm)					
	OU-6 Certified	OU-6 This work	AMH-1 Certified	AMH-1 This work	GBPG-1 Certified	GBPG-1 This work
Sc	22.1	23.1	13.48	14.6	13.93	15.2
V	129.35	131	106.4	112	96.5	97
Cr	70.78	73.8	40.89	42.3	181.4	173
Ni	39.83	40.1	32.36	36.2	59.6	58
Ba	477.24	493	322.3	332	908	912
Rb	120.2	121	18.31	18.3	56.24	54.7
Sr	130.89	133	545.4	558	363.5	353
Y	27.35	26.4	16.44	15.3	18	17.5
Th	11.51	11.64	2.64	2.63	11.23	12.45
U	1.96	2.05	0.89	0.90	0.9	0.94
Pb	28.22	28.4	9.85	9.0	14.1	13.1
Nd	29.01	29.2	17.69	17.2	43.3	43.7
Ta	1.06	1.34	0.64	0.73	0.4	0.49
Zr	174.15	177	146	147	231.8	262
Hf	4.7	4.94	3.7	3.73	6.07	6.64
La	33	33.8	15.87	16.8	52.95	53.8
Nb	14.79	16.5	8.32	9.2	9.9	10.9
Ce	74.42	76.7	33.03	33.7	103.2	102
Pr	7.8	7.96	4.21	4.28	11.45	12.07
Sm	5.92	6.05	3.68	3.91	6.79	6.90
Eu	1.36	1.34	1.16	1.21	1.79	1.83
Gd	5.27	5.69	3.34	3.65	4.74	5.45
Tb	0.85	0.84	0.51	0.50	0.6	0.63
Dy	4.99	4.95	2.84	2.75	3.26	3.14
Ho	1.01	1.04	0.57	0.57	0.69	0.67
Er	2.98	3.13	1.52	1.58	2.01	2.09
Tm	0.44	0.44	0.21	0.22	0.3	0.30
Yb	3	3.05	1.37	1.36	2.03	2.02
Lu	0.45	0.47	0.21	0.21	0.31	0.31

Note: OU-6 from GeoPT9, AMH-1 form GeoPT5 and GBPG-1 from GeoPT7 (an international proficiency test for analytical geochemistry laboratories).

References

Blichert-Toft, J., Frey, F.A., Albarède, F., 1999. Hf isotope evidence for pelagic sediments in the source of Hawaiian Basalts. Science 285, 879–882.

Carpentier, M., Chauvel, C., Maury, R.C., Mattielli, N., 2009. The "zircon effect" as recorded by the chemical and Hf isotopic compositions of Lesser Antilles forearc sediments. Earth Planet. Sci. Lett. 287, 86–99.

Chauvel, C., Lewin, E., Carpentier, M., Arndt, N., Marini, J., 2008. Role of recycled oceanic basalt and sediment in generating the Hf–Nd mantle array. Nat. Geosci. 1, 64–67.

Dai, L.Q., Zhao, Z.F., Zheng, Y.F., Li, Q., Yang, Y., Dai, M., 2011. Zircon Hf–O isotope evidence for crust–mantle interaction during continental deep subduction. Earth Planet. Sci. Lett. 308, 224–244.

Engebretson, D.C., Cox, A., Gordon, R.G., 1985. Relative motions between oceanic and continental plates in the Pacific basins. Geological Society of America Special Paper 206, 1–59.

Fan, W.M., Guo, F., Wang, Y.J., Zhang, M., 2004. Geochemistry of late Mesozoic volcanism in the northern Huaiyang tectono-magmatic belt, central China: partial melts from a lithospheric mantle with subducted continental crust relicts beneath the Dabie orogen? Chem. Geol. 209, 27–48.

Gao, S., Ling, W., Qiu, Y., Lian, Z., Hartmann, G., Simon, K., 1999. Contrasting geochemical and Sm–Nd isotopic compositions of Archean metasediments from the Kongling high-grade terrain of the Yangtze craton: evidence for cratonic evolution and redistribution of REE during crustal anatexis. Geochim. Cosmochim. Acta 63, 2071–2088.

Gao, S., Rudnick, R.L., Xu, W.L., Yuan, H.L., Liu, Y.S., Walker, R.J., Puchtel, I.S., Liu, X., Huang, H., Wang, X.R., Yang, J., 2008. Recycling deep cratonic lithosphere and generation of intraplate magmatism in the North China Craton. Earth Planet. Sci. Lett. 270, 41–53.

Guo, F., Fan, W.M., Wang, Y.J., Lin, G., 2001. Late Mesozoic mafic intrusive complexes in North China Block: constraints on the nature of subcontinental lithospheric mantle. Phys. Chem. Earth A 26, 759–771.

Guo, F., Fan, W.M., Wang, Y.J., Zhang, M., 2004. Origin of early Cretaceous calc-alkaline lamprophyres from the Sulu orogen in eastern China, implications for enrichment processes beneath continental collisional belt. Lithos 78, 291–305.

Guo, F., Nakamura, E., Fan, W.M., Kobayoshi, K., Li, C.W., 2007. Generation of Palaeocene adakitic andesites by magma mixing; Yanji area, NE China. J. Petrol. 48, 661–692.

Guo, F., Guo, J., Wang, C.Y., Fan, W.M., Li, C.W., Zhao, L., Li, H.X., Li, J.Y., 2013a. Formation of mafic magmas through lower crustal AFC processes — an example from the Jinan gabbroic intrusion in the North China Block. Lithos 179, 157–174.

Guo, J.T., Guo, F., Wang, C.Y., Li, C.W., 2013b. Crustal recycling processes in generating the early Cretaceous Fangcheng basalts, North China Craton, New constraints from mineral chemistry, oxygen isotopes of olivine and whole-rock geochemistry. Lithos 170–171, 1–16.

Hanyu, T., Tatsumi, Y., Nakai, S.I., Chang, Q., Miyazaki, T., Sato, K., Tani, K., Shibata, T., Yoshida, T., 2006. Contribution of slab melting and slab dehydration to magmatism in the NE Japan arc for the last 25 Myr: constraints from geochemistry. Geochemistry Geophysics Geosystems 7, Q08002. http://dx.doi.org/10.1029/2005GC001220.

Hermann, J., Spandler, C.J., 2008. Sediment melts at sub-arc depths: an experimental study. J. Petrol. 49, 717–740.

Hofmann, A.W., 1997. Mantle geochemistry: the message from oceanic volcanism. Nature 385, 219–229.

Jackson, M.G., Dasgupt, R., 2008. Compositions of HIMU, EM1, and EM2 from global trends between radiogenic isotopes and major elements in ocean island basalts. Earth Planet. Sci. Lett. 276, 175–186.

Jicha, B.R., Singer, B.S., Brophy, J.G., Fournelle, J.H., Johnson, C.M., Beard, B.L., Lapen, T.J., Mahlen, N.J., 2004. Variable impact of the subducted slab on Aleutian Island Arc magma sources: evidence from Sr, Nd, Pb, and Hf isotopes and trace element abundances. J. Petrol. 45, 1845–1875.

Johnson, M.C., Plank, T., 1999. Dehydration and melting experiments constrain the fate of subducted sediments. Geochem. Geophys. Geosyst. 1. http://dx.doi.org/10.1029/1999GC000014.

Kessel, R., Schmidt, M., Ulmer, P., Pettke, T., 2005. Trace element signature of subduction-zone fluids, melts and supercritical liquids at 120–180 km depth. Nature 437, 724–727.

Knudsen, T.L., Griffin, W.L., Hartz, E., Andresen, A., 2001. In-situ hafnium and lead isotope analyses of detrital zircons from the Devonian sedimentary basin of NE Greenland: a record of repeated crustal reworking. Contrib. Mineral. Petrol. 141, 83–94.

Li, S.G., Xiao, Y.L., Liou, D.L., Chen, Y.Z., Ge, N.J., Zhang, Z.Q., Sun, S.S., Cong, B.L., Zhang, R.Y., Hart, S.R., Wang, S.S., 1993. Collision of the North China and Yangtze blocks and formation of coesite-bearing eclogites: timing and process. Chem. Geol. 109, 89–111.

Li, X.H., Li, Z.X., Wingate, M.T.D., Chung, S.L., Liu, Y., Lin, G.C., Li, W.X., 2006. Geochemistry of the 755 Ma Mundine Well dyke swarm, northwestern Australia: part of a Neoproterozoic mantle superplume beneath Rodinia? Precambrian Res. 146, 1–15.

Li, X.H., Li, W.X., Li, Q.L., Wang, X.C., Liu, Y., Yang, Y.H., 2010. Petrogenesis and tectonic significance of the 850 Ma Gangbian alkaline complex in South China: evidence from in situ zircon U–Pb dating, Hf–O isotopes and whole-rock geochemistry. Lithos 114, 1–15.

Ludwig, K.R., 2001. User's Manual for Isoplot/Ex (rev.2.49): A Geochronological Toolkit for Microsoft Excel. Berkeley Geochronology Center (Special Publication, 55 p.).

Ma, L., Jiang, S.Y., Hofmann, A.W., Dai, B.Z., Hou, M.L., Zhao, K.D., Chen, L.H., Li, J.H., Jiang, Y.H., 2014. A consequence of rapid lithospheric thinning beneath the North China Craton? Geochim. Cosmochim. Acta 124, 250–271.

Macdonald, R., Hawkesworth, C.J., Heath, E., 2000. The Lesser Antilles volcanic chain: a study in arc magmatism. Earth Sci. Rev. 49, 1–76.

Martin, H., Smithies, R.H., Rapp, R., Moyen, J.F., Champion, D., 2005. An overview of adakite, tonalite–trondhjemite–granodiorite (TTG) and sanukitoid: relationships and some implications for crustal evolution. Lithos 79, 1–27.

Menzies, M.A., Xu, Y.G., Zhang, H.F., Fan, W.M., June 2007. Integration of geology, geophysics and geochemistry: a key to understanding the North China Craton. Lithos 96, 1–21.

Nakamura, H., Iwamori, H., 2013. Generation of adakites in a cold subduction zone due to double subducting plates. Contrib. Mineral. Petrol. 165, 1107–1134.

Nebel, O., Vroon, P.Z., van Westrenen, W., Iizuka, T., Davies, G.R., 2011. The effect of sediment recycling in subduction zones on the Hf isotope character of new arc crust, Banda arc, Indonesia. Earth Planet. Sci. Lett. 303, 240–250.

Nichols, G.T., Wyllie, P.J., Stern, C.R., 1994. Subduction zone melting of pelagic sediments constrained by melting experiments. Nature 371, 785–788.

Othman, D.B., White, W.M., Patchett, J., 1989. The geochemistry of marine sediments, island arc magma genesis, and crust–mantle recycling. Earth Planet. Sci. Lett. 94, 1–21.

Prelević, D., Jocob, D.E., Foley, S.F., 2013. Recycling plus: a new recipe for the formation of Alpine–Himalaya orogenic mantle lithosphere. Earth Planet. Sci. Lett. 362, 187–197.

Proyer, A., Rolfo, F., Zhu, Y.F., Castelli, D., Compagnoni, R., 2013. Ultrahigh-pressure metamorphism in the magnesite + aragonite stability field: evidence from two impure marbles from the Dabie–Sulu UHPM belt. J. Metamorph. Geol. 31, 35–48.

Qi, L., Hu, J., Conrad, G.D., 2000. Determination of trace elements in granites by inductively coupled plasma mass spectrometry. Talanta 51, 507–513.

Rapp, R.P., Watson, E.B., 1995. Dehydration melting of metabasalt at 8–32 kbar: implications for continental growth and crust–mantle recycling. J. Petrol. 36, 891–931.

Richards, A., Argles, T., Harris, N., Parrish, R., Ahmad, T., Darbyshire, F., Draganits, E., 2005. Himalayan architecture constrained by isotopic tracers from clastic sediments. Earth Planet. Sci. Lett. 236, 773–796.

Shirey, S.B., Hanson, G.N., 1984. Mantle derived Archaean monzodiorites and trachyandesites. Nature 310, 222–224.

Sun, S.S., McDonough, W.F., 1989. Chemical and isotopic systematics of oceanic basalts, implications for mantle composition and processes. In: Saunders, A.D., Norry, M.J. (Eds.), Magmatism in the Ocean Basins, 42. Geological Society of London, pp. 313–345 (Special Publications).

Tatsumi, Y., Ishizaka, K., 1982. Origin of high-magnesian andesites in the Setouchi volcanic belt, southwest Japan, I. Petrographical and chemical characteristics. Earth Planet. Sci. Lett. 60, 293–304.

Taylor, S.R., McLennan, S.M., 1985. The Continental Crust, Its Composition and Evolution. Blackwell, Oxford p. 312.

Tollstrup, D., Gill, J., 2005. Hafnium systematics of the Mariana arc: evidence for sediment melt and residual phases. Geology 33, 737–740.

Valley, J.W., 2003. Oxygen isotopes in zircon. In: Hanchar, J.M., Hoskin, P.W.O. (Eds.), Zircon. Reviews to Mineralogy and Geochemistry, 53, pp. 343–385.

Vervoort, J.D., Blichert-Toft, J., Patchett, P.J., Albarede, F., 1999. Relationships between Lu–Hf and Sm–Nd isotopic systems in the global sedimentary system. Earth Planet. Sci. Lett. 168, 79–99.

Vervoort, J.D., Plank, T., Prytulak, J., 2011. The Hf–Nd isotopic composition of marine sediments. Geochim. Cosmochim. Acta 75, 5903–5926.

Wang, W., Wang, F., Chen, F.K., Zhu, X.Y., Xiao, P., Siebel, W., 2010. Detrital zircon ages and Hf–Nd isotopic composition of Neoproterozoic sedimentary rocks in the Yangtze Block: constraints on the deposition age and provenance. J. Geol. 118, 79–94.

Weaver, B.L., 1991. The origin of ocean island basalt end-member compositions: trace element and isotopic constraints. Earth Planet. Sci. Lett. 104, 381–397.

White, W.M., Patchett, J., 1984. Hf–Nd–Sr-isotopes and incompatible element abundances in island arcs; implications for magma origins and crust–mantle evolution. Earth Planet. Sci. Lett. 67, 167–185.

Wu, F.Y., Lin, J.Q., Wilde, S.A., Zhang, X.O., Yang, J.H., 2005. Nature and significance of the Early Cretaceous giant igneous event in eastern China. Earth Planet. Sci. Lett. 233, 103–119.

Wu, F.Y., Yang, Y.H., Xie, L.W., Yang, J.H., Xu, P., 2006. Hf isotopic compositions of the standard zircons and baddeleyites used in U–Pb geochronology. Chem. Geol. 234, 105–126.

Xia, Q.K., Liu, J., Liu, S.C., Kovács, I., Feng, M., Dang, L., 2013. High water content in Mesozoic primitive basalts of the North China Craton and implications on the destruction of cratonic mantle lithosphere. Earth Planet. Sci. Lett. 361, 85–97.

Xie, L.W., Zhang, Y.B., Zhang, H.H., Sun, J.F., Wu, F.Y., 2008. In situ simultaneous determination of trace elements, U–Pb and Lu–Hf isotopes in zircon and baddeleyite. Chin. Sci. Bull. 53, 1565–1573.

Xu, S., Okay, A.I., Sengör, A.M.C., Su, W., Liu, Y., Jiang, L., 1992. Diamond from Dabie Shan eclogites and its implication for tectonic setting. Science 256, 80–82.

Xu, W.L., Zhou, Q.J., Pei, F.P., Yang, D.B., Gao, S., Li, Q.L., Yang, Y.H., 2013. Destruction of the North China Craton, delamination or thermal/chemical erosion? Mineral chemistry and oxygen isotope insights from websterite xenoliths. Gondwana Res. 23, 119–129.

Yang, J.H., Chung, S.L., Zhai, M.G., Zhou, X.H., 2004. Geochemical and Sr–Nd–Pb isotopic compositions of mafic dikes from the Jiaodong Peninsula, China: evidence for vein-plus-peridotite melting in the lithospheric mantle. Lithos 73, 145–160.

Yang, Y.H., Wu, F.Y., Wilde, S.A., Liu, X.M., Zhang, Y.B., Xie, L.W., Yang, J.H., 2009. In situ perovskite Sr–Nd isotopic constraints on the petrogenesis of the Ordovician Mengyin kimberlites in the North China Craton. Chemical Geology 264, 24–42.

Ye, K., Ye, D.N., Cong, B.L., 2000. The possible subduction of continental material to depths greater than 200 km. Nature 407, 734–736.

You, C.F., Castillo, P.R., Gieskes, J.M., Chan, L.H., Spivackm, A.J., 1996. Trace element behavior in hydrothermal experiments: implications for fluid processes at shallow depths in subduction zones. Earth Planet. Sci. Lett. 140, 41–52.

Zhang, H.F., Sun, M., Zhou, X.H., Fan, W.M., Zhai, M.G., Ying, J.F., 2002. Mesozoic lithospheric destruction beneath the North China Carton, evidence from major-, trace-element and Sr–Nd–Pb isotope studies of Fangcheng basalts. Contrib. Mineral. Petrol. 144, 241–253.

Zhang, S.B., Zheng, Y.F., Wu, Y.B., Zhao, Z.F., Gao, S., Wu, F.Y., 2006. Zircon U–Pb age and Hf–O isotope evidence for Paleoproterozoic metamorphic event in South China. Precambrian Res. 151, 265–288.

Zhao, Z.F., Zheng, Y.F., Zhang, J., Dai, L.Q., Li, Q.L., Liu, X.M., 2012. Syn-exhumation magmatism during continental collision: evidence from alkaline intrusives of Triassic age in the Sulu orogen. Chem. Geol. 328, 70–88.

Zheng, Y.F., 2012. Metamorphic chemical geodynamics in continental subduction zones. Chem. Geol. 328, 5–48.
Zheng, Y.F., Fu, B., Gong, B., Li, H., 2003. Stable isotope geochemistry of ultrahigh pressure metamorphic rocks from the Dabie–Sulu orogen in China: implications for geodynamics and fluid regime. Earth Sci. Rev. 62, 105–161.
Zindler, A., Hart, S., 1986. Chemical geodynamics. Annu. Rev. Earth Planet. Sci. 14, 493–571.
Zhou, J.B., Wilde, S.A., Zhao, G.C., Zheng, C.Q., Jin, W., Zhang, X.Z., Cheng, H., 2008a. SHRIMP U–Pb zircon dating of the Neoproterozoic Penglai Group and Archean gneisses from the Jiaobei Terrane, North China Craton, and their tectonic implications. Precambrian Res. 160, 323–340.
Zhou, J.B., Wilde, S.A., Zhao, G.C., Zheng, Y.F., Zheng, C.Q., Jin, W., Zhang, X.Z., Cheng, H., 2008b. SHRIMP U–Pb zircon dating of the Wulian complex: defining the boundary between the North and South China Cratons in the Sulu Orogenic Belt, China. Precambrian Res. 162, 559–576.
Zhou, J.B., Wilde, S.A., Zhao, G.C., Zheng, Y.F., Zheng, C.Q., Jin, W., Zhang, X.Z., Cheng, H., 2008c. SHRIMP U–Pb detrital zircon dating of low-grade metamorphic rocks in the Sulu UHP belt: evidence for overthrusting of the North China block above the South China block during continental subduction. J. Geol. Soc. Lond. 165, 423–433.
Zhou, J.B., Wilde, S.A., Liu, F.L., Han, J., 2012. Zircon U–Pb and Lu–Hf isotope study of the Neoproterozoic Haizhou Group in the Sulu orogen: provenance and tectonic implications. Lithos 136–139, 261–281.